Eur. Phys. J. B **44**, 145–167 (2005)
DOI: 10.1140/epjb/e2005-00110-y

THE EUROPEAN PHYSICAL JOURNAL B

First principles studies of the dependence of magnetism on the crystal phase in 4d and 5d late transition metals

E. Hüger[1] and K. Osuch[2,3,a]

[1] Institute of Physics and Physical Technology, Technical University Clausthal, 38678 Clausthal-Zellerfeld, Germany
[2] Department of Physics, University of South Africa, Unisa 0003, South Africa
[3] Faculty of Physics, Warsaw University of Technology, Koszykowa 75, 00-662 Warszawa, Poland

Received 28 July 2004 / Received in final form 24 December 2004
Published online 20 April 2005 –

Abstract. We investigate the possibility of inducing ferromagnetic order in $4d$ and $5d$ late transition metals through crystal symmetry change. First principles, self-consistent density functional theory calculations, with spin-orbit coupling included, performed at 0 K show that ferromagnetism occurs in the bulk of Rh and Pd at the optimum lattice constant if Rh is in the bcc and Pd in the hcp/dhcp phase. The ferromagnetic order originates in the d-band occupancy of Rh or Pd which locates the Fermi energy at the top of the highest peak of the respective (paramagnetic) density of states induced by the bcc or hcp/dhcp structure. This peak in the density of states is caused by flat bands which lie at the surface of the respective Brillouin zone. For a bcc crystal these flat bands have the e_g character and are positioned at the surface of the bcc Brillouin zone along the N-P line. The origin of the flatness of the bands was found to be the translation symmetry of the cubic lattice which causes the bands with the e_g character to be narrow along the k-lines whose k-vector directions are furthest off the directions to which the orbitals of the e_g symmetry point. Due to the d-band occupancy of Rh these flat bands lie in the paramagnetic state at the Fermi energy, whereas in the ferromagnetic state they exhibit the largest energetic split. This indicates that a smaller degree of orbital overlap narrows electronic bands enhancing the tendency of the system for ferromagnetic band split. For the hcp/dhcp structure the states contributing to the high density of para-magnetic states at the Fermi level of Pd lie in the vicinity of the M-L line of the hcp Brillouin zone boundary, which possesses a high number of symmetry (M and L) points. Moreover, the M-L line is aligned with the stacking sequence direction ([0001]) which is furthest off the densest-packed atomic chain direction of an hcp-crystal and, consequently, the weakest-bond direction in the crystal. This makes the narrow bands along the M-L line flat. The instability of the bcc and the meta-stability of the hcp crystal phase modifications for metals with native close-packed crystal structures is subsequently analysed in order to find whether they can be grown as films on suitable substrates.

PACS. 61.50.Ah Theory of crystal structure, crystal symmetry; calculations and modeling – 71.15.Mb Density functional theory, local density approximation, gradient and other corrections – 71.20.Be Transition metals and alloys – 75.50.Cc Other ferromagnetic metals and alloys

1 Introduction

A particularly well studied physical property of bulk transition metals that reflects peculiarities of their electronic structure, is the ferromagnetic order of the elemental $3d$ metals Fe, Co and Ni. Except Cr, which is known to order antiferromagnetically, and Mn, which displays a non-collinear order of its spin moments, the other $3d$ metals have a spin symmetric electronic structure. A criterion which predicts the existence of ferromagnetic order on the grounds of non-ferromagnetic (i.e. paramagnetic) properties is the so-called Stoner criterion. The Stoner criterion [1] for ferromagnetism: $I \cdot N(E_F) > 1$, where I is the Stoner parameter and $N(E_F)$ is the density of states (DOS) at the Fermi-level, tests whether the potential energy gain through the exchange interaction by establishing ferromagnetic spin alignment overcomes the energy cost of the rearrangement of the band occupation [2,3]. Thus, ferromagnetism basically occurs because of the spatial localisation of d-orbitals at the top of the d-band. This localisation produces both a large density of states and a relative maximum of the exchange integral I. The product $I \cdot N(E_F)$ is large enough for ferromagnetism to occur at the end of the $3d$ series, but not for the $4d$ and $5d$ series because the $4d$ and $5d$ wave functions extend further away from the nucleus (i.e. the $4d$ function possesses one more node than the $3d$ function). This implies a larger

[a] e-mail: osuchk@science.unisa.ac.za

interaction between the neighbour atoms in 4*d* and 5*d* metals, a larger bandwidth and thus a smaller density of states preventing the 4*d* and 5*d* metals from developing ferromagnetic order [1–4].

In compounds magnetism is less common in 4*d* and 5*d* than in 3*d* and 4*f* materials because the on-site Stoner and Coulomb parameters are lower, while the band widths W tend to be larger for the former materials due to the more extended nature of the 4*d* and 5*d* orbitals relative to the 3*d* ones. However, when it does occur it may be more interesting than typical 3*d* magnetism. In particular, the more extended active orbitals make it much more likely for itinerant electrons to play an important role in such materials, leading to interesting new phenomena such as strong coupling to lattice degrees of freedom. Furthermore, much stronger spin-orbit effects may be expected compared with 3*d* systems. They may manifest themselves in unusually strong magneto-crystalline and magneto-optical effects. In particular, an interesting example are peroskovite derived ruthenates, which display a fascinating variety of magnetic and electronic states, often with experimental signature of strong coupling to the lattice [5].

Concerning the elemental 4*d* metals Delin et al. [6,7] and Stepanyuk et al. [10] have recently pointed out on the grounds of density functional theory (DFT) calculations that although Pd and Rh are non-magnetic in their bulk structure, bridges in quantum point contacts constructed from these elements can be ferromagnetically ordered. In the present article we will show that ferromagnetic order can also occur in bulk Pd and Rh even at the optimum lattice constant if their crystal symmetries are changed. Although the DOS in 4*d* metals is reduced by the stronger interaction of 4*d* wave functions, the change of crystal symmetry can still raise the DOS at the Fermi level sufficiently enough to fulfil the Stoner criterion for ferromagnetism.

The article is organised as follows. In Section 2 we point out that fcc, bcc, hcp and dhcp (double-hcp) phase modifications of late transition and noble metals can be experimentally realised in the form of thin films grown on suitable substrates. Section 3 presents experimental evidence confirming theoretically predicted ferromagnetic order in Rh and Pd clusters. The calculation procedure presented in Section 4 will be applied in Section 5 to analyse the effect of crystal phase change on the electronic structure of all 4*d* and 5*d* late transition metals. It will be demonstrated that the change of crystal symmetry from natural fcc into bcc induces ferromagnetic order in Rh whereas the change from fcc to hcp/dhcp induces ferromagnetic order in Pd at the optimum lattice constant. This will be attributed to the position of the Fermi level at the top of the strongest peak of the bcc or hcp/dhcp DOS for Rh or Pd, respectively. Section 6 is devoted to the explanation of the occurrence of those strong peaks in the DOS of bcc Rh and hcp/dhcp Pd. We will demonstrate there that the symmetry at a k-point (translation + point group symmetry) is responsible for flat bands which, in turn, lead to strong peaks in the bcc and hcp DOS. Section 7 discusses the instability/metastability of the bcc and hexagonal (hcp/dhcp) phase modifications of metals whose native structure is close-packed, showing how such metals can be grown in the form of thin epitaxial films possessing the corresponding phase modification. Our conclusions will be summarised in Section 8.

2 Crystal phase modifications

In contrast to lattice dilated metals [11,12] and free standing monolayers (MLs) of late transition metals [13,14], for which calculations predict the existence of ferromagnetic order but which cannot be experimentally realised [15], the fcc, bcc, hcp and dhcp crystal phase modifications of late transition and noble metals can be stabilised in the form of thin films deposited on suitable substrates [18–42]. Metals whose natural phase is bcc or hcp can be grown in the (100)-oriented fcc (or fct) phase modification via pseudomorphic growth [16] on (100)-oriented cubic metals. The best known examples are: the growth of up to 60 MLs thick (100)-oriented fcc films of Fe on Cu(100) [18–20], of (100) and of up to 700 ML of (110)-oriented fcc films of Co on (100)- and (110)-oriented Cu substrates [20–22] and of fcc Ti on Al(100) [23]. Metals whose natural phase is hcp or fcc have also been successfully grown [16] (via pseudomorphic growth) in the form of (100)-oriented bcc films on (100)-oriented metal substrates. Examples are: bcc (or bct [16]) Co on various (100)-oriented substrates such as Fe(100) [24, 25] and bcc Au on W(100) [26]. The hcp and dhcp crystal phase modifications of late transition and noble metals (whose natural phase is fcc) have successfully been stabilised in the form of up to 100 ML thick films deposited on suitable (100)-oriented substrates [27,28,31,32,34]. Examples are: hcp and dhcp Ni grown on Fe(100) and Au(100) [27, 28, 35] and hcp and dhcp Pd grown on W(100) or Nb(100) [27,28,31]. Also the stabilisation of the hcp phase modification of metals whose natural phase is bcc has been reported for Fe on Ru(0001) [36] and for Nb on Zr [41]. Moreover, pseudomorphic growth can stabilise thin films of rare-earth metals in crystal phase modifications. For example Eu, a bcc metal, was found to grow in the fcc phase on Re [42]. Beside the induction of phase modifications via epitaxial growth, there are experimental results showing that clusters of metals whose natural phase is fcc (like Ni) order in the hcp phase modification below the critical median size of 4 nm whereas larger particles are still fcc [43]. The stability and magnetic order of two- or three-dimensional free standing or supported clusters is an interesting area of research within which also clusters of 4*d* and 5*d* transition metals have intensively been studied.

3 Ferromagnetism in clusters of 4d late transition metals

Clusters of Ru [44], Rh [44, 45] and Pd [45, 46] have experimentally been found to be ferromagnetically ordered.

First principle calculations showed that ferromagnetic order in small Pd clusters occurs because they stabilise in a structure which breaks the four-fold symmetry of the natural fcc phase [47,48]; Pd clusters in the fcc phase are found to be non-ferromagnetic [47,48]. Recently, ferromagnetic order in Pd clusters was found to be directly related to the density of stacking faults existing in fcc Pd particles [49]. Since the occurrence of a stacking fault breaks locally the four-fold symmetry of the fcc lattice, the experimental data of Sampedro et al. [49] shows that the fraction of atoms which carry the ferromagnetic order lies in those clusters in a close-packed structure characterised by lack of four-fold symmetry.

In contrast, the magnetism of Rh clusters is not affected by this symmetry transformation when close-packed structures (fcc-cuboctahedral and icosahedral) are compared [48]. Ab initio calculations have found that Rh_4 clusters with four-fold symmetry are ferromagnetic whereas tetrahedral clusters, which have three-fold symmetry (i.e dense-packed structure), are not ferromagnetically ordered [50]. Similarly, calculations [51] and experimental results [52] showed that it is not the bulk but the surface atoms of (100)-oriented fcc Rh (which are characterised by lack of three-fold symmetry) that are ferromagnetically ordered. Thus, experimental results [44–46, 49, 52] and first principles calculations [47, 48, 50, 51] strongly indicate that the break of four-fold symmetry favours the occurrence of ferromagnetic order in Pd structures, whereas the preservation of four-fold symmetry in a non close-packed structure enhances ferromagnetic behaviour in Rh.

Using first principles DFT calculations we will confirm the suppositions made above by calculating the crystal phase dependence of the magnetic order in 4d and 5d late transition metals. We will show that ferromagnetic order can easily be explained by considering the shape of the density of states (for example the energy position of the peaks) which strongly depends on the crystal phase symmetry and not on the atomic number. Consequently, we will demonstrate that the crystal phase which preserves the close-packed structure without having four-fold symmetry, namely the hcp and dhcp structure, leads for Pd to a DOS at the Fermi energy ($N(E_F)$) high enough to induce ferromagnetic order in the metal at the equilibrium lattice constant. The situation for Rh is reversed. The crystal phase which preserves four-fold symmetry but is not close-packed, i.e. bcc, raises $N(E_F)$ for Rh to a value high enough to induce ferromagnetic order in the metal at the equilibrium lattice constant. We will discuss the origin of the flat bands (of the bulk band structure) which are responsible for the high $N(E_F)$ values of DOS in Section 6.

4 Calculation procedure

The calculations were performed within the framework of DFT, using the full potential linearised plane wave (FLAPW) method and the LSDA approximation [53, 54] as implemented in the Wien2k package [55]. First scalar relativistic calculations were carried out and subsequently spin-orbit coupling was included in a second variation step [55]. The calculations were performed at 560 k-points in the irreducible wedge of the Brillouin zone. The optimum lattice constants of the studied bulk structures were determined by minimising the total energy as a function of the lattice constant. Convergence of the self-consistent calculations was assumed when the charge distance defined as $\int |\rho_n(r) - \rho_{n-1}(r)| d^3r$, where ρ is the charge density and n is the iteration number, was smaller then 1×10^{-4}e in three consecutive iterations. It should be mentioned that LDA (LSDA) underestimates the lattice constants of transition metals [56]. Gradient corrections, on the other hand, dramatically reduce the error [56–58] and also give the correct natural phase stability [59], but they tend to overestimate the magnetic moment [3,56,62]. Since ferromagnetic order in transition metals is the prime objective of this study, we decided to use mainly the LSDA approximation.

5 Magnetic order and crystal symmetry

5.1 Ferromagnetic 3d metals

Before presenting our own results we want to briefly summarise the results obtained so far on the dependence of magnetism on the crystal phase for the well known 3d ferromagnets: Fe, Co and Ni. Iron is ferromagnetically ordered at the optimum lattice constant only in its natural bcc phase [64–66], with the magnetic moment of 2.2 μ_B per atom. Fcc Fe is in an anti-ferromagnetic state [66] and hcp Fe in a non-ferromagnetic state [65] at the optimum lattice constant. Cobalt is ferromagnetically ordered in all the three phases (i.e. hcp, fcc, bcc) at the optimum lattice constants, with bcc Co having the largest magnetic moment, followed by the moments of fcc and naturally occurring hcp Co [67]. Non-ferromagnetic order has been calculated for bcc Ni [68], whereas for hcp Ni ferromagnetic order with the magnetic moment by 0.2 μ_b per atom lower than in fcc Ni (0.6 μ_b per atom) was measured [27, 69].

To the best of our knowledge the dependence of magnetism on the crystal phase for late 4d and 5d metals has, until now, not been explored. In the following we will show that crystal phase change can be the driving force behind ferromagnetic order in bulk Pd and Rh at the optimum lattice constant.

5.2 Phase stability

Panel (a) of Figure 1 gives the total energy of Rh in the bcc, fcc, hcp and dhcp crystal structures as a function of the lattice constant. The optimum atomic densities, i.e. the densities at the lattice constants for which the total energies shown in Figure 1 attain minima, are the same for all the four crystal structures, with the optimum atomic density of fcc Rh corresponding to the nearest neighbour distance of 2.67 Å, which is by less than 1% smaller than the experimental value of 2.69 Å. Due to different symmetry and especially because of the nearest and next-nearest neighbour distances being different in the bcc and

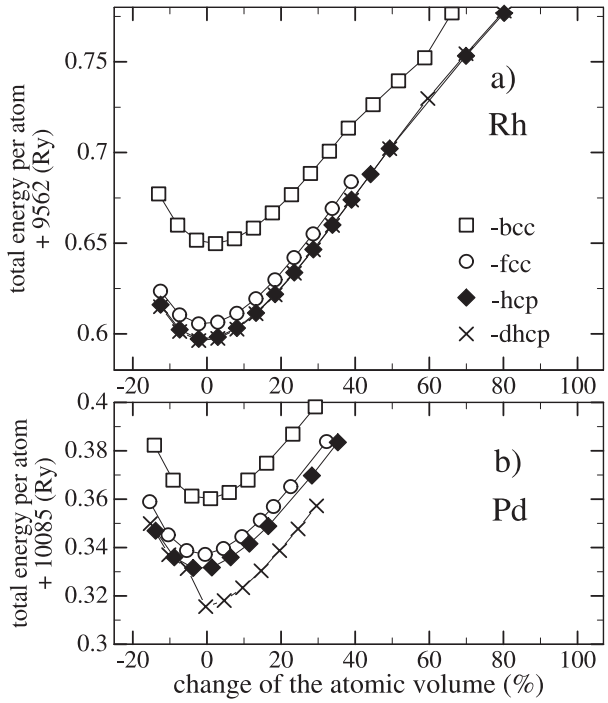

Fig. 1. Total energy of bulk Rh (panel (a)) and bulk Pd (b) in the bcc (squares), fcc (circles), hcp (diamonds) and dhcp structure (crosses) as a function of atomic volume expansion (+) or contraction (–) obtained from DFT spin-polarised calculations with spin-orbit coupling included.

fcc structures, the total energy of bcc Rh is, as expected, much higher than that of its natural fcc structure. On the other hand, the total energies of hcp and dhcp Rh are smaller than that of fcc Rh. In this context the similarity between the fcc, hcp and dhcp crystal phases, which are all close-packed structures, becomes important. The hexagonal close-packed structures (hcp, dhcp) have the same atomic nearest and next-nearest neighbour distances as the fcc structure. Since these lattices differ only in the stacking sequence of the densest-packed hexagonal atomic monolayers, they are nearly energetically equivalent. Similar results were obtained for Pd [31]. For comparison the total energies of Pd in the four crystal phases are plotted in the lower panel of Figure 1. The hexagonal phases (i.e. hcp and dhcp) of Pd have slightly lower total energies than the natural fcc phase. It should be stressed that this result is valid only at 0° K and does not mean that the hexagonal phases of Rh and Pd are energetically more favourable than their fcc phase also at finite temperatures. However, this cannot explain the marked drop of the total energy of dhcp Pd at the optimum lattice constant. Below we will show that the occurrence of ferromagnetic order can provide a suitable explanation of this effect.

The fact that our DFT calculations done at 0 K wrongly predict the hexagonal phases to be slightly more stable than the natural fcc phase is not unexpected. Although first principles calculations based on DFT are very successful in explaining many properties of materials, including some ground state properties of transition metals [3, 70–72], they often give the hcp phase to be more stable than the natural fcc or bcc phase. Many studies [60,73] have demonstrated that the energy differences between the bcc, fcc and hcp phases are very small if the *d*-band is filled. These differences increase with the decreasing *d*-band occupancy until the *d*-band occupancy of Fe is reached. Non-spin polarised self consistent calculations found the fcc phase of Fe to be by 24 mRy per atom more stable than its natural bcc phase. Furthermore, the calculations show that if bcc Fe were not ferromagnetic, Fe would have the hcp ground state [66,73,74] in full accordance with the crystal structure of Ru and Os, the 4*d* and 5*d* counterparts of Fe. The inclusion of spin-polarisation reduces the total energy of ferromagnetically ordered bcc Fe by 33.9 mRy, making bcc the most stable phase of Fe among all the other ones [66]. Note, that also ferromagnetically ordered fcc Fe has its total energy reduced, but only by some 2 mRy [66]. This different behaviour of fcc and bcc Fe was related to the locus of the Fermi level inside the *d*-bands of the spin minority states [60]. It was claimed that, similarly to the noble metals, the (almost) filled spin-majority *d*-bands of Fe contribute to smaller extent to the energy differences between various structures than the spin-minority *d*-bands. The bcc structure locates the Fermi energy for the spin-minority bands of Fe in a deep minimum of the DOS, which separates the bonding states, leaving them occupied, from the anti-bonding states which remain unoccupied [75]. This results in a strong stability of the bcc phase similar to that of the metals with nearly half-filled *d*-bands like W or Mo [66,73,75]. In the case of fcc Fe the Fermi level of the spin-minority states does not lie in a minimum like that of bcc Fe, thus only slightly reducing the total energy of fcc Fe.

It seems that a similar situation occurs also for Pd when the fcc, hcp and dhcp structures are considered. Many authors [11,12,60,66] have shown that lattice expansion produces ferromagnetic order in late transition metals. For lattice-expanded Pd a magnetic moment of up to 0.36 μ_B was reported [11,12]. As a consequence of the *d*-band occupancy of Pd, this magnetic moment makes the spin-majority *d*-bands of Pd almost completely filled. Thus, in analogy to Fe, the total energy of magnetic Pd should be strongly influenced only by the spin-minority bands. Panel (a) and (b) of Figure 2 give the paramagnetic DOS of fcc and hcp Pd near the Fermi energy, respectively. For fcc and dhcp Pd a magnetic moment of up to 0.36 μ_B would push the Fermi level of the spin-minority states to the top of a strong DOS peak. Similarly to fcc Fe, this would lead for fcc and hcp Pd to a hardly discernible drop in their total energies. For dhcp Pd the situation is different. In the paramagnetic state (Fig. 2c) the Fermi level lies at the top of one of the two strong peaks of the dhcp DOS. Similarly to bcc Fe, a spin anisotropy in dhcp Pd would shift the Fermi level of the spin-minority states exactly to the minimum between the two peaks (see Fig. 2e). As will be discussed later, peaks in the DOS are a consequence of the narrow portions of bands at the peak energy. It is well known that due to the total reflection

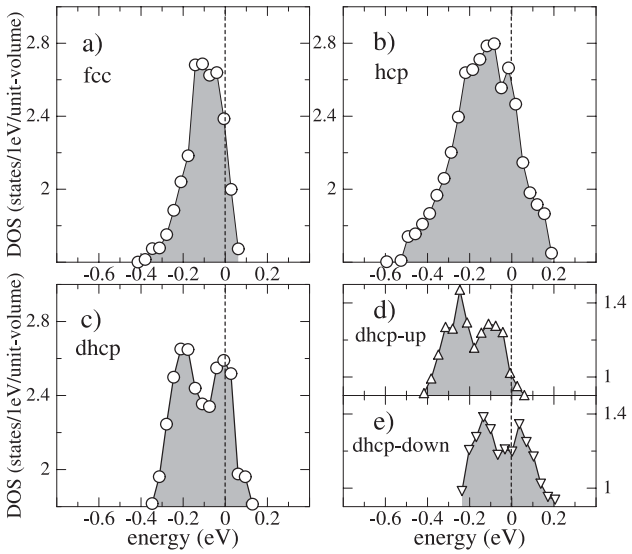

Fig. 2. (a, b, c) Paramagnetic, *d*-projected DOS of fcc Pd (panel (a)), hcp Pd (b) and dhcp Pd (c) at the optimum lattice constant obtained from DFT calculations with spin-orbit coupling included. (d, e) Spin-majority (panel (d)) and spin-minority (e) *d*-projected DOS of dhcp Pd at the optimum lattice constant obtained from ferromagnetic DFT calculations with spin-orbit coupling included. The magnetic moment is 0.11 μ_B per atom. The energy scale in this and in the next figures is given relative to the Fermi energy. Consequently the Fermi energy corresponds to zero on the scale and occupied electronic states have negative energies. The position of the Fermi energy is marked with thin vertical lines. In this and in the next figures the unit-volume represents the unit-cell volume divided by the number of atoms in the (non-primitive) unit-cell, i.e. the so-called volume per atom (atomic-volume).

of the band states at the high symmetry points of the Brillouin zone (BZ) bands become flat there. High symmetry points exist at the centre and at the edge of the BZ. For a band with mostly *d*-character the exchange energy gain at the BZ-edge will be rather large [6–9] if the band splits due to spin-polarisation in such a way that one of the spin channels ends above (Fig. 2e) and the other below the Fermi energy (Fig. 2d). As a consequence, the total energy of dhcp Pd would drop at the onset of ferromagnetic order (Fig. 1b). Thus, the drop of the total energy of dhcp Pd at the optimum lattice constant could be explained if ferromagnetic order occurred in dhcp Pd at the equilibrium lattice constant.

5.3 Occurrence of ferromagnetic order

Ferromagnetic order appears if the energy gained by a preferential parallel spin alignment surpasses the energy needed to induce the desired spin order. The energetic profit comes from the repulsive interaction between the electrons (exchange interaction). Due to the Pauli exclusion principle the probability of finding an electron in the vicinity of another electron with the same spin direction is much lower than if the electrons have opposite spins. Larger distances between electrons lead to weaker repulsive interactions between them reducing the total energy of the system. Thus the repulsive interaction between electrons favours parallel positions of the spins and with that a spontaneously magnetised state. The potential energy gain through the exchange interaction of parallel spins is proportional to the number of electrons which can be rearranged to have their spins parallel. To raise the number of electrons with one spin direction (majority spin direction) at the cost of the other spin direction (minority spin direction) the electronic system has to be changed. The electrons with the majority spins have to occupy states above the initial Fermi level. This increases the total kinetic energy of the electronic system. The increase in the kinetic energy is proportional to (i) the number of the minority spin electrons which are shifted to non-occupied (majority spin) states and (ii) the band energy difference encountered during this process [2]. On the one hand, the system gains exchange energy by introducing spin asymmetry, on the other, the induced spin-order increases the total kinetic energy of the electronic system. Thus, ferromagnetic spin alignment is favourable if a high number of (minority spin) electrons can be shifted to non-occupied (majority spin) states over a small band energy difference. Therefore, an important quantity for the occurrence of ferromagnetic order is the density of states at the Fermi level ($N(E_F)$). The Stoner criterion for ferromagnetism: $I \cdot N(E_F) > 1$, tests whether the potential energy gain through the exchange interaction by establishing ferromagnetic spin alignment overcomes the energy cost of the rearrangement of the band occupancy [2]. Since the Stoner parameter I, which is related to exchange interaction, is only insignificantly influenced by different crystal symmetries, the decisive role in establishing ferromagnetic order is played by the density of states at the Fermi energy. This is especially the case for 4*d* and 5*d* metals, where the Stoner parameter shows practically no dependence on the atomic number.

5.4 DOS and crystal structure

Calculating the electronic structure of late transition and noble metals in various crystal phases, we observe that the optimum atomic density and the related *d*-band width are independent on the crystal phase. On the other hand, the shape of the DOS (for example the position of the peaks inside the DOS) stringently depends on the crystal phase and not on the atomic number. By comparing the DOS of different crystal phases, we notice that the larger the difference in the crystal symmetry, the larger the difference in the shape of the DOS. For example, Figures 3a, b, c, d show the *d*-projected DOS of Pd in the bcc, fcc, hcp and dhcp phase. It can be observed that the DOS of the dhcp structure is a superposition of the DOS of the fcc and hcp ones, which can be attributed to the fact that the stacking sequence of the close-packed hexagonal atomic layers is for the dhcp structure positioned in between the fcc and hcp sequences. On the other hand, the DOS of the bcc phase, which does not contain

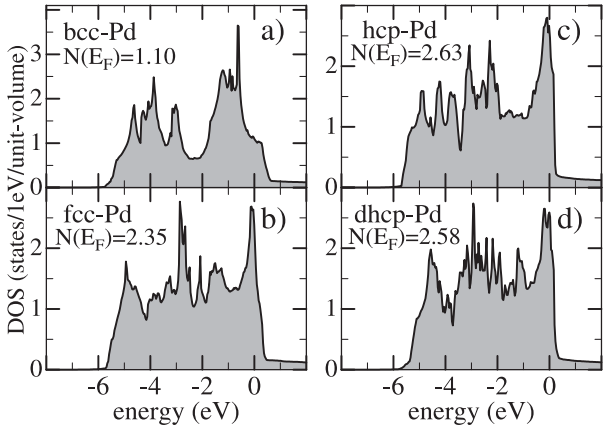

Fig. 3. Paramagnetic, d-projected DOS of bulk Pd in the bcc (a), fcc (b), hcp (c) and dhcp structure (d) at the optimum lattice constant obtained from DFT calculations with spin-orbit coupling included. (The calculated optimum lattice constant is by 1% smaller than the experimental one.)

close-packed hexagonal atomic layers, is very different from the DOS of those phases (fcc, hcp, dhcp) which contain these layers. Yet, the shape of the DOS is very similar for all the d-band metals in the same crystal phase, with the position of the Fermi level relative to the valence band being dependent on the occupancy of this band. Thus, it is sufficient to analyse the crystal phase dependence of the electronic structure of only one d-band metal, for example of Pd, to obtain useful information about the dependence of the electronic structure (for example the DOS at the Fermi level) on the crystal phase of the other d-band metals. The differences between those metals consist in the position of the Fermi energy within the DOS due to a different d-band filling and the dependence of the d-band width on the atomic number. In general, the d-band width (W) increases with the decreasing atomic number within a row of the periodic table of elements while increasing down the groups of the table ($W_{3d} < W_{4d} < W_{5d}$). Using these considerations we will now analyse the electronic and magnetic properties of $4d$ and $5d$ late transition metals.

5.4.1 Pd and Pt

The $4d$ metal Pd is not ferromagnetic although it possesses in the natural fcc phase a high DOS $N(E_F)$ of 2.35 at the Fermi energy. Therefore a popular view has been established that metallic Pd needs just a little push to become ferromagnetically ordered [76]. Bland and associates [77] supposed that the magnetic properties of Pd are sensitive to structural change because of the high DOS at the Fermi surface. As already mentioned, a change of crystal symmetry is accompanied by a change of the shape of the DOS (i.e. of the position of the maxima). Figure 3 shows that for Pd the preservation of the four-fold symmetry at the change of the crystal structure to a non-close-packed one (i.e. a structure which does not possess close-packed hexagonal atomic planes), namely bcc, significantly reduces the DOS at the Fermi level to $N(E_F) = 1.1$. We have shown [31] that ferromagnetic order does not appear in bcc Pd even when the lattice is expanded by more than 40%. In contrast, the break of the four-fold symmetry with the simultaneous preservation of the close packed structure (leading to hcp or dhcp structure) raises the DOS at the Fermi-level to $N(E_F) = 2.58$ for dhcp Pd and to $N(E_F) = 2.63$ for hcp Pd. As a consequence, ferromagnetic order appears in hcp and dhcp Pd at the optimum lattice constant (see also Fig. 5). Investigating the electronic structure of Pd films grown in the hcp/dhcp crystal structure on W(001) and Nb(001) substrates with ultraviolet photoelectron spectroscopy we found evidence of a ferromagnetic spin-split [31]. Recently, Sampedro et al. [49] have experimentally confirmed our findings showing that Pd in an hcp or dhcp environment is ferromagnetically ordered.

Pt the $5d$ counterpart of Pd, has the same valence band occupancy as Pd. Thus, analogously to Pd, the hcp phase of Pt could be of interest as far as ferromagnetic order is concerned. Unfortunately, a larger d-band width of Pt in comparison to Pd together with the fact that the Stoner parameters of 5d metals are smaller than those of $4d$ metals (which in turn are much smaller than the respective parameters of $3d$ metals) [14,78] make hcp Pt only paramagnetically ordered.

Although the electronic structure of bcc Pd (Fig. 3a) is quite insusceptible to spin anisotropy, it is nevertheless interesting as far as magnetic order is concerned. In the total DOS of bcc Pd (Fig. 3a) there exists a sharp and strong peak at the energy of -0.7 eV. It is the strongest peak out of those exhibited by the DOS of bcc, fcc, hcp and dhcp Pd. If a metal had the Fermi level there, a preferential spin alignment would very probably develop in it. Obviously, such a metal would have to have a bcc structure and a d-band occupancy with one (or a little more than one) electron less than Pd. We will further consider Rh as a possible candidate for such a metal.

5.4.2 Rh

Figures 4a, b, c, d show the paramagnetic d-projected DOS of bcc (panel (a)), fcc (b), hcp (c) and dhcp (d) Rh at the optimum lattice constants. The Fermi level intersects the DOS of bcc Rh exactly across the strongest peak, which leads to a very high DOS there (three times higher than that of fcc Rh). As a result, ferromagnetic order in bcc Rh at the optimum lattice constant is established with the magnetic moment of 0.26 μ_B (Fig. 5a). The behaviour of the total energy with lattice expansion and contraction is for the various crystal phases of Rh (Fig. 1a) similar to that of Pd (Fig. 1b). In contrast, the behaviour of the magnetic moment of Rh for these crystal phases (Fig. 5a) is completely reversed in comparison to that of Pd (Fig. 5b): bcc Rh is ferromagnetically ordered at the optimum lattice constant whereas fcc, hcp and dhcp Rh is not ferromagnetic even at the lattice expansion of up to 40%.

The behaviour of the magnetic moment can also be explained by the DOS of Rh, which is, as indicated above,

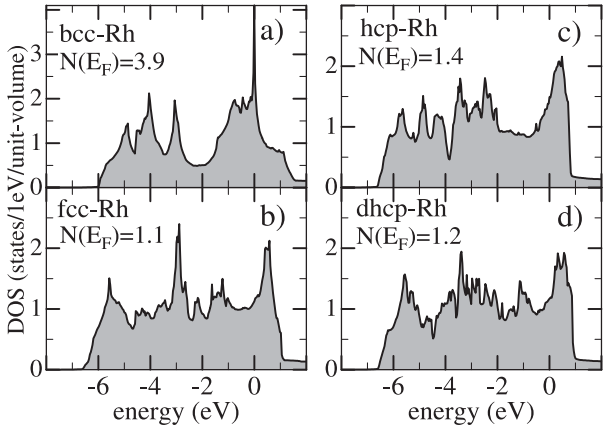

Fig. 4. Paramagnetic, *d*-projected DOS of bulk Rh in the bcc (a), fcc (b), hcp (c) and dhcp structure (d) at the optimum lattice constant obtained from DFT calculations with spin-orbit coupling included.

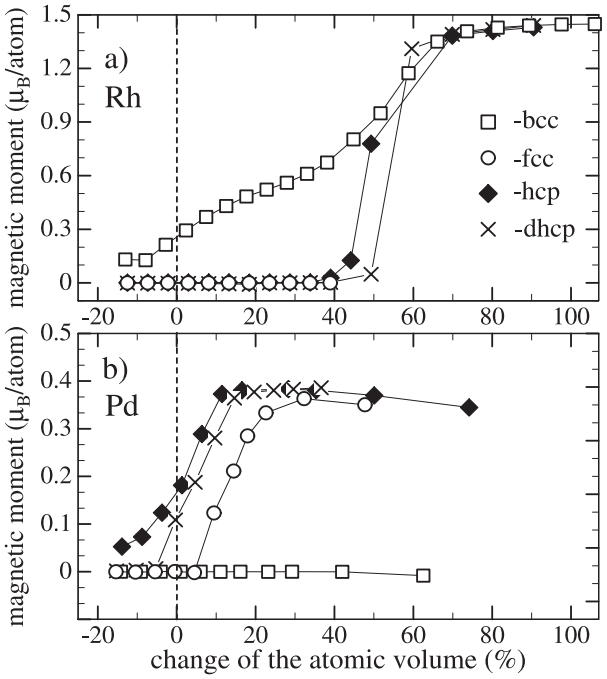

Fig. 5. Magnetic moment of bulk Rh (panel (a)) and bulk Pd (b) in the bcc (squares), fcc (circles), hcp (diamonds) and dhcp structure (crosses) as a function of atomic volume expansion (+) or contraction (–) obtained from DFT spin-polarised calculations with spin-orbit coupling included. Note that the total energy (see Fig. 1) of dhcp Rh does not drop like that of dhcp Pd at the optimum lattice constant, because dhcp Rh is not ferromagnetically ordered there and obviously the double-peak DOS structure (see Fig. 4d) lies well above the Fermi energy.

very similar to that of Pd. However, the position of the Fermi level within the DOS of Rh is different than that of Pd due to its smaller *d*-band occupancy and larger *d*-band width originating from its smaller atomic number. Comparing the DOS of Rh (Fig. 4) and Pd (Fig. 3), it can be seen that the larger *d*-band width of Rh reduces the heights of the peaks in its DOS relative to those of Pd. An exception to this behaviour is the strongest peak in the DOS of the bcc structure, whose height stays the same for the both metals. As indicated above, the position of this peak at the Fermi level of bcc Rh leads to a very high DOS there. In contrast, the position of the Fermi level of fcc, hcp and dhcp Rh leads to a small DOS at the Fermi level in these phases. Even the lattice expansion of up to 40% does not enlarge it enough to induce ferromagnetism in these phases of Rh. Further expansion induces ferromagnetic order there with the saturated value of almost 1.5 μ_B (Fig. 5a) at the expansion of 90%. This is also the value to which the magnetic moment of bcc Rh saturates. In contrast to fcc, hcp and dhcp Rh, the position of the Fermi level at the top of the strong DOS maximum induces ferromagnetic order in bcc Rh at the optimum lattice constant and maintains it even if the bcc lattice is contracted. Measurements of Tomaz et al. [79] have shown that bct Rh is ferromagnetically ordered whereas fct Rh is not, providing experimental evidence that changing the crystal structure from fcc to bcc, by introducing tetragonal distortion [81], indeed induces ferromagnetic order in Rh.

5.4.3 Ir, Ru and Os

Ir has a similar electronic structure as Rh. Having a larger *d*-band width and a smaller Stoner parameter it does not, however, exhibit ferromagnetic order at the optimum lattice constant, not even in the bcc structure.

In the case of other late transition metals like Ru and Os, their Fermi levels do not cross strong maxima of the DOS of the bcc, fcc, hcp and dhcp crystal phases. In addition, the smaller atomic numbers of Ru and Os (in comparison to Pd and Pt) work against a possible establishment of ferromagnetic order in these elements, because they dilate the *d*-band width (in comparison to that of Pd and Pt) reducing the peak heights of their DOS.

5.5 Orbital magnetic moment

In contrast to the atomic state, where orbital magnetic moments are fully developed, in the bulk they are quenched. Although spin-orbit coupling reduces the spin-related magnetic moment [80] (by lowering the DOS and by causing more spin-flips among the majority spins than among the minority spins, thus reducing the difference between spin-up and spin-down numbers) it also induces a small orbital moment by spin-polarisation. Sticht and Kübler [83] have shown that the experimental magnetic moment of Gd coincides with the theoretically determined one only when the orbital moment is added to the spin related moment. Since spin-orbit interaction is larger for 4*d* than for 3*d* metals let us see what orbital moment results from the spin-polarisation of bcc Rh and hcp/dhcp Pd at the optimum lattice constant. Ebert et al. [84] obtained a simple equation which relates orbital moment μ_{orb} to (i) spin-orbit coupling parameter (ξ),

(ii) the spin-majority ($N^{(\downarrow)}(E_F)$) and (iii) spin-minority ($N^{(\uparrow)}(E_F)$) density of states at the Fermi-energy [85]:

$$\mu_{orb} = I_z \simeq \xi[N^{(\downarrow)}(E_F) - N^{(\uparrow)}(E_F)]. \quad (1)$$

This equation gives at the equilibrium lattice constants the orbital moments per atom of $\mu_{orb}^{bcc-Rh} \simeq 0.06\ \mu_B$, $\mu_{orb}^{\mathrm{hcp-Pd}} \simeq 0.07\ \mu_B$ and $\mu_{orb}^{\mathrm{dhcp-Pd}} \simeq 0.06\ \mu_B$ for bcc Rh, hcp Pd and dhcp Pd, respectively. These values are smaller than the respective spin-moments, but positive, leading at the optimum lattice constants to the total magnetic moments per atom of ($\mu_{tot} = \mu_{spin} + \mu_{orb}$), $\mu_{tot}^{\mathrm{bcc-Rh}} = 0.32\ \mu_B$, $\mu_{tot}^{\mathrm{hcp-Pd}} = 0.23\mu_B$, $\mu_{tot}^{\mathrm{dhcp-Pd}} = 0.16\ \mu_B$ for bcc Rh, hcp Pd and dhcp Pd, respectively.

Summarising this section, we found that the four-fold symmetry in a non close-packed structure favours ferromagnetic order in bulk Rh at the optimum lattice constant, whereas the lack of four-fold symmetry in a close-packed structure favours the appearance of ferromagnetism in bulk Pd. This conclusion can offer a possible explanation for a lower magnetic moment obtained for Rh nanowires in comparison to Pd nanowires in a calculation at the nanowire equilibrium bond length. Despite the expectation that in lower dimensions Rh should have a larger magnetic moment than Pd due to the former having more empty d-bands than the latter, Delin and Tossatti [7] calculated for Rh nanowires a magnetic moment of 0.3 μ_B and for Pd nanowires a larger magnetic moment of 0.7 μ_B at the nanowire equilibrium bond length. It should be noted, however, that to simulate the nanowires the authors used an inherently three-dimensional code [8]. Therefore, the infinitely long nanowires were arranged in an infinite two-dimensional hexagonal array. So, their three-dimensional lattice was a hexagonal one which was stretched considerably in-plane (i.e. parallel to the hexagonal planes) to properly reduce the interaction between the nanowires lying perpendicularly to the hexagonal planes. The wire-wire vacuum distance was set to at least three bond lengths and the bond-length in the nanowire was allowed to relax, which, due to the in-plane extension of the system, resulted in a bond-length smaller than the atomic nearest neighbour distance in the natural fcc crystal phase. Now, a speculative explanation of the lower magnetic moment obtained for Rh nanowires in comparison to Pd ones can be the symmetry of the 3-dimensional lattice used in the calculation. Although the 3-dimensional lattice was considerably expanded in-plane, it was still characterised by lack of four-fold symmetry which, according to our conclusion above, should: (i) enhance the magnetic moment of Pd, and to (ii) reduce it for Rh, in agreement with the results of Delin and Tossatti [7].

6 The origin of flat bands

The fact that only 3d late transition metals show ferromagnetic order in their natural crystal phases can be explained in a simple way by large values of the respective Stoner parameters and the relation of their atomic numbers to the d-band widths. Being each at the top of a transition metal group (3d instead of 4d or 5d) with the largest atomic number within the 3d-row of transition metals, Fe, Co and Ni have the narrowest d-bands of all of these metals, which insures the highest possible DOS at the Fermi level. Beside having smaller Stoner parameters, the 4d transition metals (with the narrowest d-band width within the 4d row) have broader d-band widths than their counterparts in the 3d metal group which decrease the height of the DOS maxima for Ru, Rh, Pd in comparison to Fe, Co and Ni. In consequence, ferromagnetic order does not develop in the natural crystal phases of the 4d metals. However, the d-band widths of Rh and Pd are still narrow enough to produce the DOS at the Fermi level high enough for ferromagnetic order to develop if Rh is in the bcc and Pd in the hcp or dhcp phase, respectively. In contrast to their counterparts in the 5d row (Ir and Pt) (which have broader d-band widths and therefore smaller DOS maxima than Rh and Pd) ferromagnetism develops in these phases of Rh and Pd in their bulk structure at the optimum lattice constants. Because the ferromagnetic order is strongly related to the Fermi energies lying at the top of the strongest peaks in the DOS of the bcc and hcp/dhcp structures, we will further search for the origin of those peaks. This will be done by identifying the band states in the bulk band structure which give rise to the DOS peaks mentioned above. After that we will discuss the origin of these states by relating them to the symmetry of the respective crystal structure.

6.1 The origin of the strongest peak in the bcc DOS

Figure 6 shows the calculated paramagnetic DOS of bcc Rh within the LSDA (Figs. 6a, b) or GGA (Fig. 6c) approximation with (Figs. 6a, c) or without (Fig. 6b) spin-orbit coupling included. In all the cases a strong peak at the Fermi energy is present. It is worth noting that the peak becomes even higher if the GGA approximation is used or spin-orbit coupling is not included. Such a peak occurs not only for Rh or Pd, but also in the bcc DOS of all the transition metals [3, 4, 86, 87]. Andersen [87, 88] has shown that within the atomic sphere approximation (ASA) canonical d-bands may be derived that depend only on the crystal structure (that is, they depend neither on the lattice constant nor on the particular transition metal). The bcc DOS derived from the canonical d-bands is also characterised by a strong peak, which for the d-band occupancy of Rh lies at the Fermi energy (Fig. 6). A similar peak also appears in the DOS calculated for metals in the bcc lattice within the hybrid nearly-free electron tight-binding secular equation [89]. All these results show that the strong peak at the Fermi level of the DOS of bcc-Rh DOS is characteristic of the bcc crystal lattice. Let us now see how it can be accounted for.

6.1.1 Points of symmetry in k-space

In a crystalline solid, the motion of electrons is characterised by energy bands $E_n(k)$ with band index n and

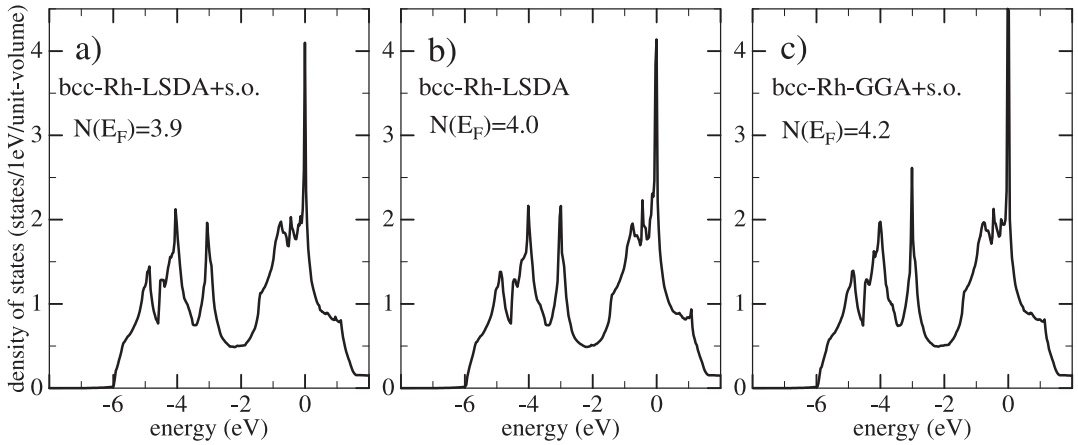

Fig. 6. *d*-projected DOS of bulk Rh in the bcc structure at the optimum lattice constant obtained from DFT non-spin-polarised calculations within the LSDA (panels (a, b)) or GGA approximation (c), with (a, c) or without (b) spin-orbit coupling included.

wave vector k. DOS (which gives the number of electronic states as a function of energy) involves summation (integration) over all the wave vectors. Thus the occurrence of a peak in DOS means that states at many (different) points in momentum space (i.e. at many irreducible k-vectors) have energy equal to that of the peak. This happens when flat bands exist at that energy. Due to the lattice symmetry, bands become flat at symmetry points of the bulk Brillouin zone (bulk BZ). The bulk BZ, which is related to the periodicity of a crystal in the momentum space, delimits the region in this space which contains all the irreducible wave vectors. Due to the symmetry of the lattice, the bulk BZ possesses, beside the centre of the BZ (Γ point), points of symmetry only at the BZ boundaries. Panel (a) of Figure 7 shows the BZ of the bcc structure which possesses, beside the centre (Γ), three points of symmetry at the BZ surface: H, N and P [90]. Figures 8 and 9 present the bulk band structure of bcc Rh in the crystallographic high symmetry directions $\langle 100\rangle$ (Γ-H), $\langle 110\rangle$ (Γ-N) and $\langle 111\rangle$ (Γ-P) in the paramagnetic (Fig. 8) and ferro-magnetic (Fig. 9) state. It can be observed (Fig. 8) that the bcc symmetry locates states with k at the symmetry points N and P at the Fermi energy, forming there a flat band between these points (i.e. in the N-P direction). This band appears in all the bcc transition metals and is also present in the bcc canonical bands [4, 86, 87]. Figure 10 demonstrates that the flat band along the N-P line also appears in the bcc structure of transition metals whose natural phase is different from the bcc one. Thus the symmetry of the bcc lattice must be at its origin.

Figure 7 shows that the NP line is the symmetry axis D of the bcc BZ. It lies on the surface of the BZ in the $\langle 100\rangle$ direction at the intersection of the ΓNP and NPH symmetry plane (the latter being at the surface of the bcc BZ). The thick dashed lines in panel (b) of Figure 7 show a cube whose edges are made up of the P-N segments. Interestingly, all states situated on the surface of this cube have a periodicity in the momentum space which is two times smaller than that of the other states which possess the periodicity of the fcc lattice, which is the reciprocal lattice of

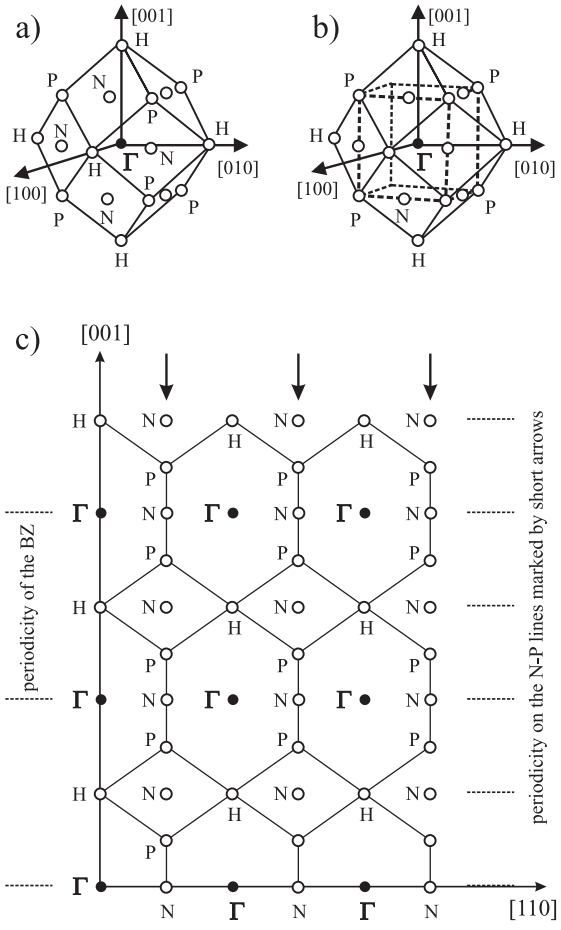

Fig. 7. (a) Brillouin zone of the bcc lattice. (b) Inserted in the bcc BZ is a cube (marked with the thick dashed lines) whose corners are symmetry points P and edges are on the N-P line situated on the surface of the bcc BZ. (c) {110} (ΓNPH) plane cut through the extended zone scheme of the bcc BZ. The length of the k-vectors on the N-P lines (D-symmetry axis) marked with short arrows and aligned with the $\langle 001\rangle$ direction is two times smaller than of those lying on the k-lines aligned with the $\langle 001\rangle$ direction.

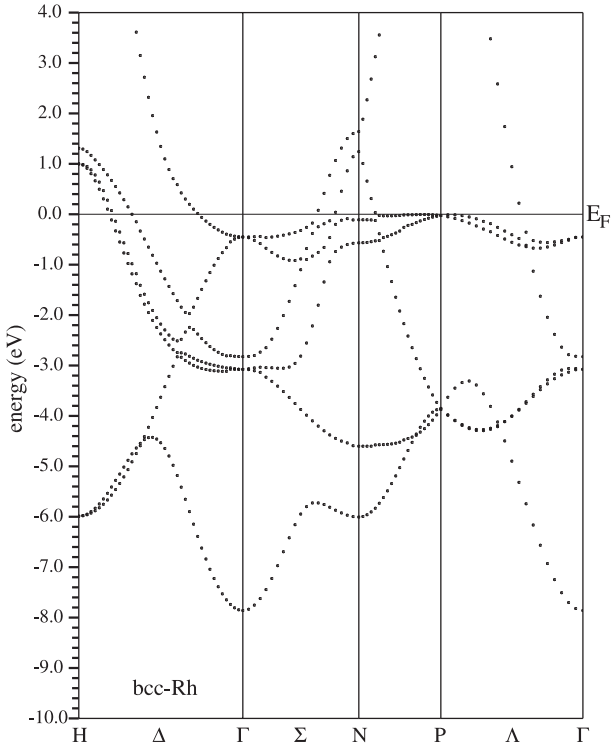

Fig. 8. Bulk band structure of bcc Rh along the crystallographic high symmetry directions: $\langle 100 \rangle$ (Γ-H), $\langle 110 \rangle$ (Γ-N), and $\langle 111 \rangle$ (Γ-P) obtained from a paramagnetic LSDA calculation with spin-orbit coupling included performed at the equilibrium lattice constant of bcc Rh.

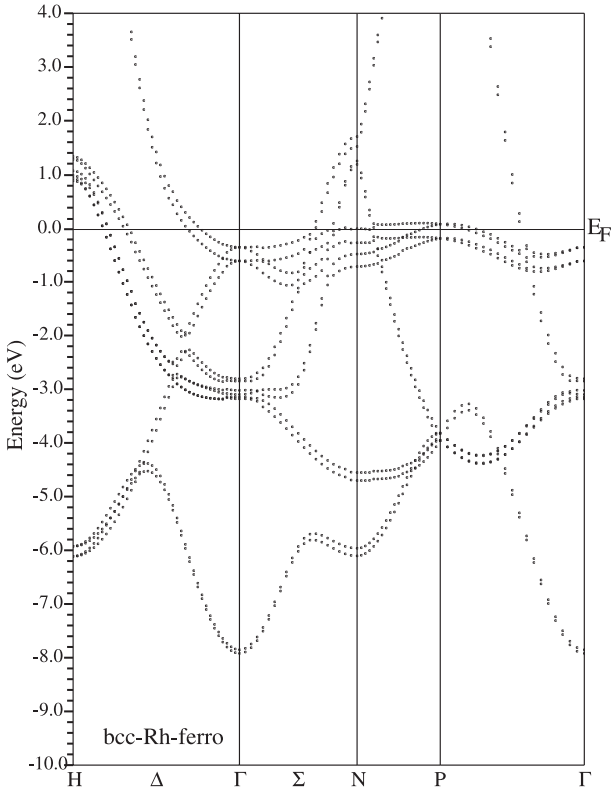

Fig. 9. Ferromagnetic (spin-up and spin-down) bulk band structure of bcc Rh, showing a small, k-point and energy dependent band-split. Notice that the band-split is larger for bands which are narrow and lie in the vicinity of the Fermi energy. For the origin of these bands see Section 6.1.2. The bands were obtained from spin-polarised LSDA calculation with spin-orbit coupling included performed at the equilibrium lattice constant of bcc Rh.

the bcc crystal. This is illustrated in panel (c) of Figure 7. The periodicity on the NP line (e.g. the line marked with the short arrows in Fig. 7c)) is two times smaller than the periodicity on the ΓH line which is parallel to the NP line. It could be supposed that the origin of the flatness of the band at the Fermi energy between points N and P arises from the abundance of symmetry points N and P on the NP line.

Deng, Simon and Köhler [91] have recently obtained the necessary and sufficient condition for the occurrence of a 'flat band' at an arbitrary point in momentum space. They found two factors which lead to a 'flat band'; one of which is k-dependent, and the other k-independent. The k-dependent part is related to the existence of a third order pseudo-inversion centre at a k-point. A third order pseudo-inversion centre means that inversion symmetry holds only for three directions defined by linearly independent vectors, not necessarily for all possible directions as for a real centre. The pseudo-inversion centre also refers to the situation where only approximate symmetry exists due to structure modulation or distortion. Now, unfortunately, all the points between points N and P of the bcc BZ do not satisfy this requirement. Deng, Simon and Köhler [91] have shown that even when k-points are not third order pseudo-inversion centres a band can still be flat due to the k-independent part which refers to weak covalent bonding. A weak covalent bond between atoms of different cells leads to a small group velocity, thus producing a flat band.

Figure 11 shows the difference between the self-consistent electronic and the atomic charge densities in the densest packed atomic plane (bcc-{110}) of bcc Nb. It thus indicates where the electronic charge moves upon bonding. The continuous lines represent charge density increase, whereas the dashed lines denote charge density depletion. From that contour-plot it can be observed that the strongest bond exists between the nearest neighbour atoms lying in the $\langle 111 \rangle$ direction which is the atomic densest-packed direction of a bcc crystal. The bonds are weaker in all directions off the $\langle 111 \rangle_{bcc}$ direction, being the weakest in the $\langle 100 \rangle_{bcc}$ direction. It can also be observed that there is electronic charge density depletion only between the atoms exactly in this direction. Thus, the flatness of the band along the N-P line could be explained as follows. As the N-P line has $C_{2\nu}$ (mm2) symmetry, only a second order pseudo-inversion centre exists on it. The k-points on this line are all extremal points with respect to lines in the {100} plane, while along the $k_{\langle 100 \rangle}$ direction there is no pseudo-inversion centre, so $\partial E_k / \partial k_{\langle 100 \rangle} \neq 0$. As the interatomic bonding in the $\langle 100 \rangle_{bcc}$ direction is rather weak, the group velocity in

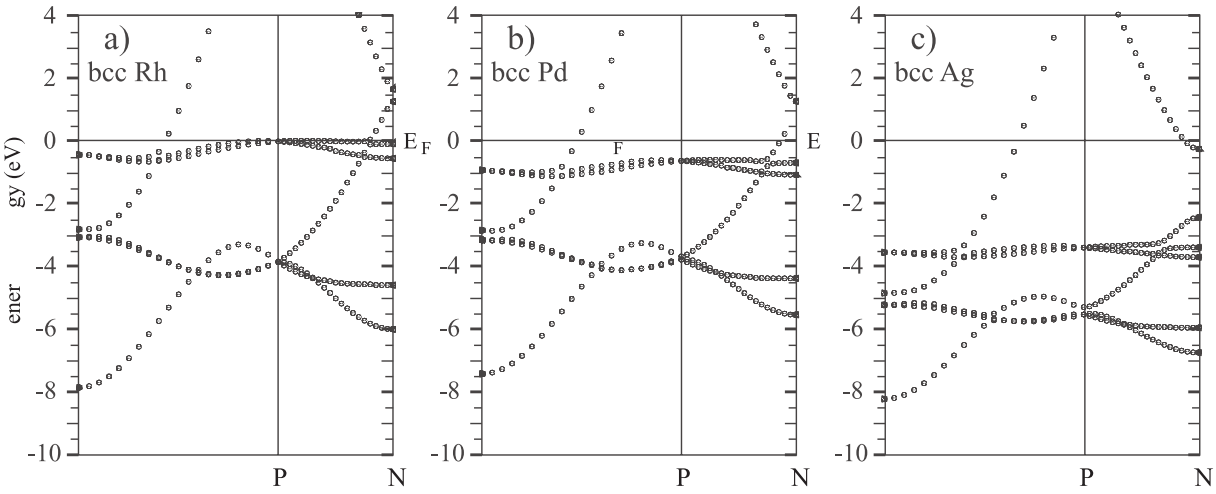

Fig. 10. Band structure of bcc Rh (panel (a)), bcc Pd (b) and bcc Ag (c) along the Γ-P-N direction. The LSDA approximation was used and spin-orbit coupling was included. Note that although the band width decreases with the atomic number, the spin-orbit coupling induced splitting of states (e.g. those located for Rh at Γ at -2.8 eV and -3 eV) increases with the atomic number (i.e. from Rh to Pd and then to Ag).

that direction, $\partial E_k/\partial k_{\langle 100\rangle}$, is very small. In this way we could tentatively explain the flatness of the band along the N-P line as arising from symmetry (second order pseudo-inversion centre) and weak bonds in the $\langle 100\rangle_{bcc}$ direction. However, on the grounds of this explanation all the bands along the line should be flat. Yet, as Figure 8 shows, this is not the case: only the band at the Fermi energy is flat. The other bands even exhibit considerable dispersion (step-bands) in that direction. Similarly, the k-points on the $\Gamma - H$ line are second-order pseudo-inversion centres and at the same time they are extremal points with respect to lines in the $\{100\}$ plane, while in the $k_{\langle 100\rangle}$ direction there is no pseudo-inversion centre, so $\partial E_k/\partial k_{\langle 100\rangle} \neq 0$. However, a small group velocity in the $\langle 100\rangle_{bcc}$ direction, would cause the bands along the $\Gamma - H$ line to be flat. To the contrary, as it is seen in Figure 8 there are no flat bands along this line. Therefore, another explanation of the flatness of the band situated in the N-P direction has to be found.

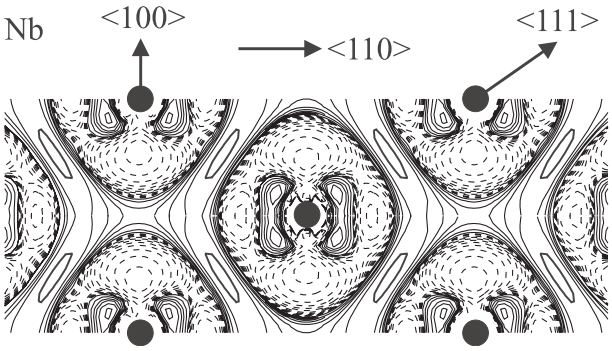

Fig. 11. Difference between the self-consistent electronic charge density of bcc Nb and the superposition of atomic charge densities. The presented contour plot is a $\{110\}$ plane-cut through Nb. Solid lines indicate a charge density increase, whereas dashed lines a charge density decrease. The positions of atomic nuclei are given by the black circles.

6.1.2 Translation symmetry in real space

Obviously band dispersion appears when the band energy changes with the changing k-vector of a band-state. The energy of the band state is directly related to the magnitude of the wave function at the unit-cell boundaries [92, 93]. The larger the amplitude of the wave function between atoms (i.e. a unit-cell boundary), the larger the binding energy (which is negative) of the state. A maximum of the wave function between atoms corresponds to a 'bonding' and a minimum (node) to an 'antibonding' character of the state. Thus, the occurrence of band dispersion means that the magnitude of the wave function at the unit cell boundaries also changes with a changing k-vector. Consequently, lack of band dispersion (i.e. a flat band) on a k-line means that for the k-vectors ending on that line the magnitudes of the wave functions on the cell boundaries do not change with changing k.

To relate the change of the k-vector to the change of the wave-function on the unit-cell boundary we will use the well known [93] intuitive explanation of the appearance of band dispersion for states in solids. This will be done by considering the translation symmetry of Bloch functions and the orbital character of Bloch factors. Due to translation symmetry, wave functions in solids have the Bloch form: $\psi(\mathbf{k},\mathbf{r}) = u(\mathbf{k},\mathbf{r})e^{i\mathbf{kr}}$, where $u(\mathbf{k},\mathbf{r})$ is the Bloch factor with the property: $u(\mathbf{k},\mathbf{r}+\mathbf{R}) = u(\mathbf{k},\mathbf{r})$ for all primitive translations $\mathbf{R}$. Now, when the whole crystal is translated by $\mathbf{R}$, the Bloch function gets multiplied by $e^{i\mathbf{kR}}$. Although the general case is a little difficult to consider, we can easily see what the effect of this factor is for the centre of the BZ ($k = 0$) and for its edge ($k = \pi/R$). For $k = 0$ the factor $e^{ikR} = 1$ and the translation does not change the wave function. For $k = \pi/R$, $e^{ikR} = e^{\pi i} = -1$

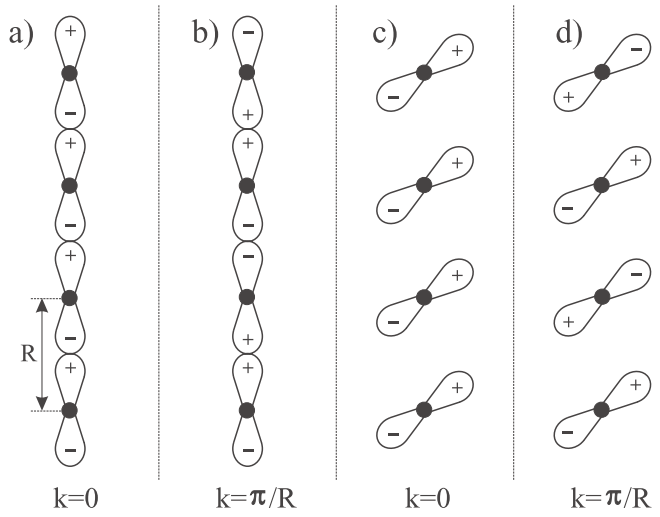

Fig. 12. Rough representation of the Bloch functions at the BZ centre ($k = 0$) (panels (a, c)) and at the BZ boundary ($k = \pi/R$) (b, d) along an atomic chain. The positions of atomic nuclei are marked with the dots and the interatomic distance is equal to R. In panels (a, b) the orbitals point in the direction of the atomic chain, whereas in (c, d) they point off this direction. The translation symmetry does not change the value of the wave function in the mid-points between atoms for $k = 0$. For $k = \pi/R$ the magnitude of the Bloch function is significantly changed in the mid-points between atoms only when the orbitals point along the chain. In panel (a) the Bloch function possesses a minimum between atoms whereas in panel (b) it has maxima there. As a consequence $E^{b)}(k = \pi/R) > E^{a)}(k = 0)$ and the band between $k = 0$ and $k = \pi/R$ exhibits dispersion becoming a step-band. For the case where the orbitals do not point in the direction of the atomic chain, the energy of the states at $k = 0$ and $k = \pi/R$ does not differ much. The further off the atomic chain direction the orbitals point, the closer are the energies of the states at $k = 0$ and $k = \pi/R$ ($E^{d)}(k = \pi/R) \simeq E^{c)}(k = 0)$), and consequently, the narrower is the band.

and the wave function changes its signature at the translation from one atom to the other. This has important implications for the magnitude of the wave function in between atoms when the orbitals point in the direction of an atomic chain and is illustrated in Figure 12. If this is the case, then for $k = 0$ (Fig. 12a) there are nodes of the wave function at the nuclei and at the mid-points between them. In contrast, for $k = \pi/R$ there are nodes only at the nuclei (Fig. 12b) and, as a consequence, $E(k = 0) < E(k = \pi/R)$. For k between $k = 0$ and $k = \pi/R$ the energy values are, in most cases, in the range between $E(k = 0)$ and $E(k = \pi/R)$ and the band has dispersion. Now, since in the case of Figures 12c, d the orbitals do not point in the direction of the atomic chain, the change of the wave function due to translation symmetry will not significantly affect its behaviour between atoms and, consequently, $E(k = 0) \sim E(k = \pi/R)$. Thus, band dispersion appears when orbitals are directed toward atoms, whereas when they point away from atoms bands are narrow (flat), in perfect agreement with the results obtained for $4d$ and $5d$ metal nanowires by Delin et al. [6–9]. It follows from their calculations, in which the atomic wires were parallel to the z-axis, that the bands whose orbitals point along atomic chains, i.e. the bands with the $d_{3z^2-r^2}$ orbital character have the largest energy dispersion (see for example Fig. 4 in Delin, Tossatti and Weht [6]). On the other hand, the bands with the $d_{xz,yz}$ orbital character, whose orbitals points 45 degrees off the atomic chain direction, exhibit smaller energy dispersion. The narrowest bands are those with the $d_{x^2-y^2}$ and d_{xy} character, whose orbitals point furthest off the atomic chain direction, being perpendicular to those chains. We will now apply this conclusion to the bcc bulk band structure.

For the cubic structure the crystallographic $\langle 100 \rangle$ directions is furthest off the crystallographic $\langle 110 \rangle$ and $\langle 111 \rangle$ directions. It follows, that the bands with symmetry e_g should display the largest dispersion along lines of k-vectors in the $\langle 100 \rangle$ direction, because the orbitals with symmetry e_g (i.e. $d_{x^2-y^2}$ and $d_{3z^2-r^2}$) point in that direction. The further off that direction k-vectors of a line are, the narrower a band along this line should be. Since the orbitals of states with symmetry t_{2g} (i.e. d_{xy}, d_{xz} and d_{yz}) point in the $\langle 110 \rangle$ direction, the bands with this symmetry should show the largest dispersion along the $\langle 110 \rangle$ direction. The further off that direction k-vectors of a line are, the narrower a band along the line should be. Thus, in the directions where the orbital overlaps are small the band dispersion should be rather small. As it is further shown, these conclusions apply to the bcc bulk band structure.

The m-resolved character of the bcc bands is shown in Figures 13−17. In these figures, orbital character $d_{x^2-y^2}$, $d_{3z^2-r^2}$, d_{xy}, d_{xz} and d_{yz}, respectively, is proportional to the size of the circles. At the centre Γ of the BZ there should only be two levels, since in a cubic environment orbitals d_{xy}, d_{xz}, d_{yz} (t_{2g}) are equivalent and orbital $d_{x^2-y^2}$ is, in fact, also equivalent to orbital $d_{3z^2-r^2}$ (symmetry e_g). One of the levels should comprise orbitals d_{xy}, d_{xz}, d_{yz} (t_{2g}) and be therefore triply degenerate, and the other orbitals $d_{x^2-y^2}$ and $d_{3z^2-r^2}$, and be doubly degenerate. This is observed in Figures 13−17 (the state at −7.85 eV is of s and not of d character), with the difference that states t_{2g} split off in two (also three-fold) degenerate levels due to spin-orbit interaction (Fig. 10 shows that the band split is larger for Ag than for Pd and, in turn, for Pd larger than for Rh). The t_{2g} and e_g degeneracy is lifted outside Γ. The band dispersions fully comply with the considerations above. The bands with symmetry e_g have the largest dispersion along the Δ axis (Γ-H line) because its k-vectors are aligned with the direction to which the orbitals of the e_g states point. They are narrow along the Γ-N-P-Γ line because its k-vectors are directed off the $\langle 100 \rangle$ direction, to which the orbitals of symmetry e_g point. In contrast, the dispersion of the bands with symmetry t_{2g} is weaker along the k-line parallel to the $\langle 100 \rangle$ direction (i.e. the Γ-H line) than along the Γ-N-P-Γ line because the k-vectors of the former line are aligned with the $\langle 100 \rangle$ direction which is furthest off the direction into which the orbitals of t_{2g} symmetry point (i.e. $\langle 110 \rangle$).

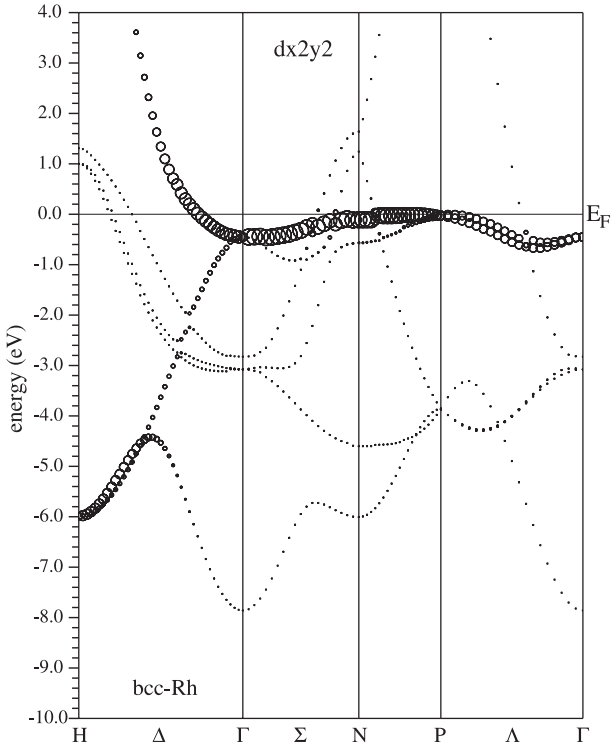

Fig. 13. The same as in Figure 8 but now with $d_{x^2-y^2}$ character represented by the size of the circles.

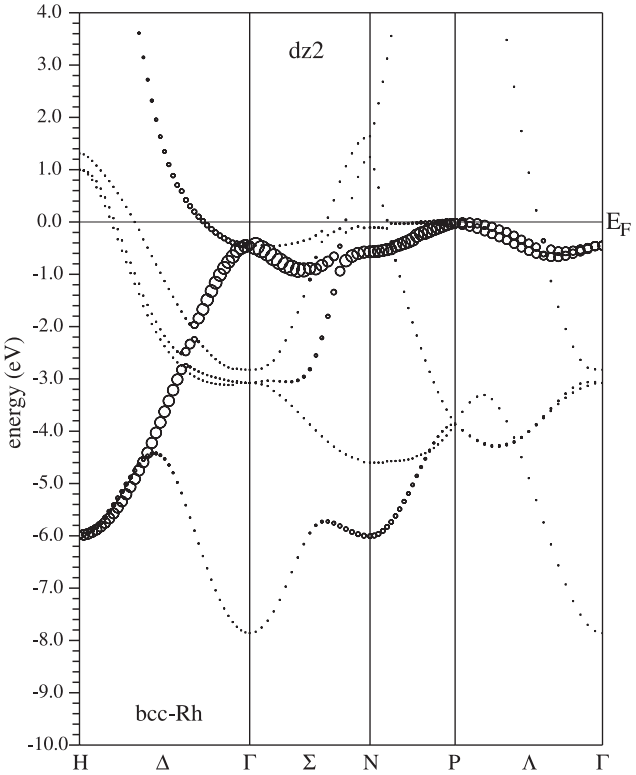

Fig. 14. The same as in Figure 8 but now with $d_{3z^2-r^2}$ character represented by the size of the circles.

6.1.3 Atomic density along crystallographic directions

It can also be observed that bands t_{2g} have larger dispersion than bands e_g: along the k-lines where the bands have the largest dispersion (the Γ-N line for bands t_{2g} and the Γ-H line for bands e_g) as well as along the k-lines where the bands have the smallest dispersion (the Γ-H line for bands t_{2g} and the Γ-N-P-Γ line for bands e_g) the dispersion of bands t_{2g} is larger than of those whose symmetry is e_g. This can be explained by taking into account not only the cubic symmetry but also the atomic density along the various crystallographic directions. In the bcc structure the densest-packed direction is the $\langle 111 \rangle$ direction. Consequently, the strongest bonds in the bcc metals occur in this direction (see Fig. 11) and the weakest – furthest off it, i.e. in the $\langle 100 \rangle$ direction (Fig. 11). Because orbitals t_{2g} point into a direction ($\langle 110 \rangle$-direction) which is much closer to the $\langle 111 \rangle$ direction, than that of orbitals e_g, which point exactly into the direction of the weakest bonds between atoms (the $\langle 100 \rangle$ direction), the bands with symmetry t_{2g} should, in general, exhibit stronger dispersions than bands with symmetry e_g, exactly as shown in Figures 13−17. The weaker bonds in the $\langle 100 \rangle$ direction result in bands e_g being flat along the N-P line, because only the N-P line is aligned with the direction of the weakest bonds (i.e. $\langle 100 \rangle$). This is especially the case for the states with symmetry $d_{x^2-y^2}$ which make up a flat band along N-P line situated at the Fermi level. The states with character $d_{3z^2-r^2}$ do not form a fully flat band there because, in contrast to orbitals $d_{x^2-y^2}$, orbitals $d_{3z^2-r^2}$ also extend

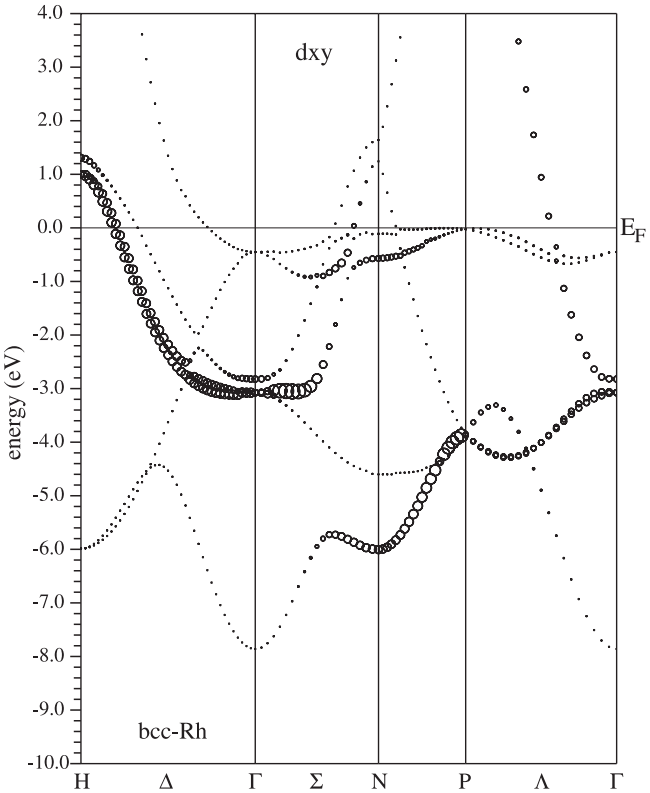

Fig. 15. The same as in Figure 8 but now with d_{xy} character represented by the size of the circles.

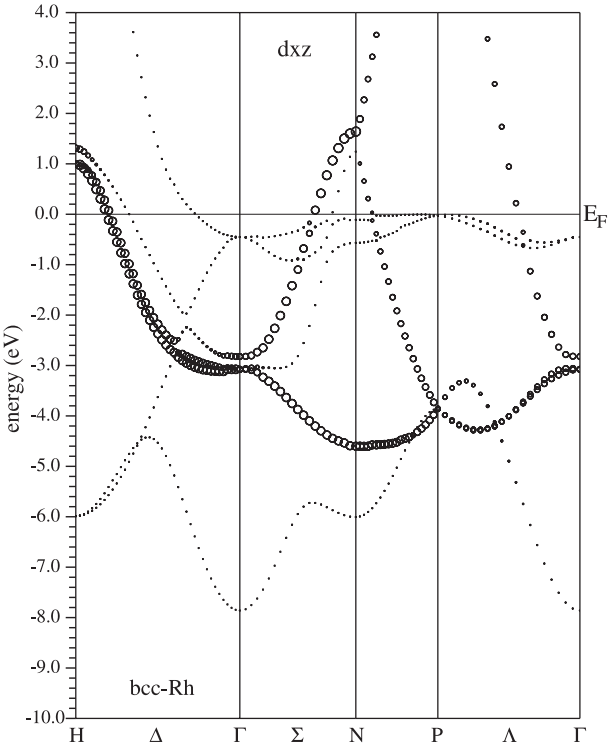

Fig. 16. The same as in Figure 8 but now with d_{xz} character represented by size of the circles.

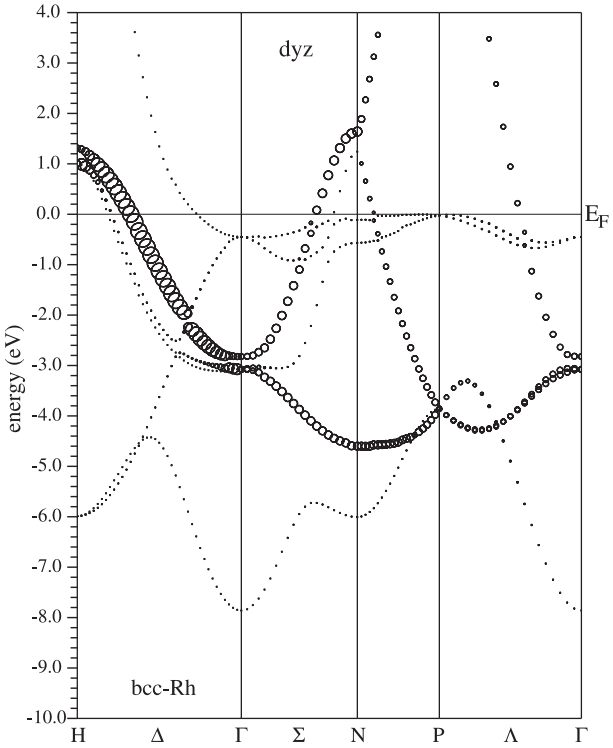

Fig. 17. The same as in Figure 8 but now with d_{yz} character represented by the size of the circles.

a little into the (100) plane, thus pointing slightly off the direction ([001]) of the weakest bonds.

Figure 18 shows the l- and m-resolved DOS of bcc Rh at the optimum lattice constant. It clearly indicates that the strong peak in the bcc DOS is made up of states with symmetry e_g, i.e. of states with character $d_{3z^2-r^2}$ (Fig. 18d) and especially with $d_{x^2-y^2}$ (Fig. 18c), confirming the considerations above. Figure 9 shows that the flatness of the bands with the predominant e_g orbital character is for Rh strongly correlated with the appearance of ferromagnetic order. The ferromagnetic band split is stronger (see Fig. 9) for bands with the e_g orbital character in the vicinity of the Fermi energy, where they are narrow (Figs. 13–17). Clearly, the tendency to ferromagnetic band split is enhanced for these bands by a smaller orbital overlap which narrows the bands.

Summarising Section 6.1, we found that the strongest peak of the bcc DOS is produced by the flat bands of symmetry e_g lying mostly on the N-P line. The origin of these bands was found to be the translation symmetry of the cubic structure which makes the bands with symmetry e_g narrow along a k-line whose k-vectors are off the $\langle 100\rangle$-directions, e.g. on the Γ-N-P-Γ line. This happens because the magnitude of the wave function between atoms does not change significantly with varying k-vectors of this k-line. In addition, the bands are flatter along the N-P line because of the highest abundance of symmetry points on it and because the N-P direction is aligned with the $\langle 100\rangle$ direction, which is the direction of the weakest bonds in the bcc crystal. According to a recent itinerant theory of magnetism, a ferromagnetic state is stabilised at low enough temperatures, if an almost dispersion-less band exists within broad ones [94]. Thus the flat band touching the Fermi energy plays a leading role in the formation of the magnetic state.

6.2 The origin of the strongest peak in hcp Pd

In a recent letter [31] we identified the flat bands which raise the DOS at the Fermi energy of hcp Pd as lying at the surface of the hcp bulk Brillouin zone in the stacking sequence direction ($\langle 0001\rangle$), which is the most remote direction from the densest-packed atomic chains $\langle 1\bar{1}00\rangle$ of the close packed structure. Blaha, Schwartz and Dederichs [95] have shown that the bonds in the stacking sequence direction are for hcp transition metals weaker than those within the close-packed hexagonal (0001) planes. This happens also for Ti which has the hcp c/a ratio of 1.58, which is smaller than the ideal one of $c/a \simeq 1.63$. For hcp Pd the hexagonal c/a ratio was calculated [96] to be even larger (1.68) than the ideal one. In general, it has been found that the hcp phase of those metals whose fcc phase is stable with respect to hcp, is characterised by an increased axial ratio [97]. First principles calculations performed at conserved atomic densities [72] lead to the conclusion that the total energy minimum of hcp Au and Ag occurs at the c/a value of 1.67. For hcp/dhcp Pd and hcp Cu films grown on W(100) [27, 28, 31] and for hcp/dhcp Pd and Au, and hcp Cu and Ag films grown on Nb(100) [27, 28, 31, 32, 98] we measured the c/a value of $\sim$1.67 and an atomic nearest neighbour distance (lattice constant a) smaller by $\sim 1\%$,

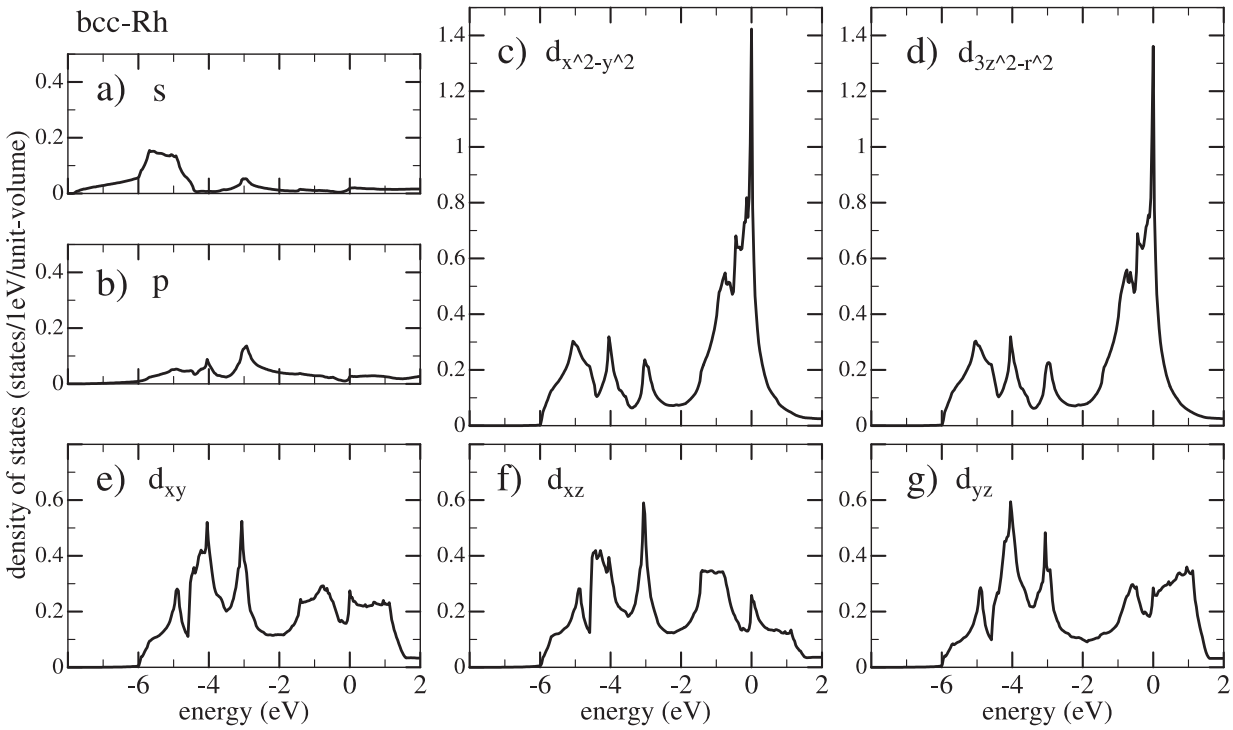

Fig. 18. *l*- and *m*-resolved DOS of bcc Rh at the optimum lattice constant obtained from paramagnetic DFT calculations using the LSDA approximation with spin-orbit coupling included. a) *s*-projected DOS. b) *p*-projected DOS. c) $d_{x^2-y^2}$, d) $d_{3z^2-r^2}$, e) d_{xy}, f) d_{xz} and g) d_{yz} contributions to the DOS.

which leaves the atomic density unchanged. This reflects the fact that atomic bonds in the hcp phase modification for metals whose natural phase is fcc (e.g. for Pd) are stronger within the (0001) atomic plane and weaker in the stacking sequence direction (i.e. [0001]). Thus for hcp/dhcp Pd the strongest peak positioned at the Fermi energy is produced by flat bands lying along the M-L line on the surface of the hcp BZ in the [0001] direction where (i) in the momentum space there exist a high abundance of symmetry points and (ii) in the real space the bonds between atoms are the weakest.

7 Structural phase transition

In the preceding sections the relation between the magnitude of the DOS at the Fermi energy of late transition metals and their crystal structure was analysed. We will now investigate the implications of a high density of states at the Fermi energy of those metals for the instability of their lattices. This will be done to the end of exploiting the possibility of producing substrate supported or even free-standing, thick films of Pd and Rh with the bcc and/or hcp crystal phase.

7.1 The influence of a flat band at the Fermi-energy on the crystal phase stability

The existence of an electronic flat band at the Fermi level plays a crucial role in a metal becoming a ferromagnet or a superconductor [91,99–105]. However, the resulting high electronic density of states at the Fermi energy ($N(E_F)$) corresponds rather to a relatively unstable situation since already weak perturbations, for example very small volume fluctuations, may trigger off the rearrangement of a large number of electrons [106]. The system avoids such an instability by a spin anisotropy or by a phase transition to a more stable crystal structure. As is shown in Figure 9, the bands which are narrow in the vicinity of the Fermi energy have the largest ferro magnetic band-split. In the case of Co, a metal isoelectronic to Rh, Liu and Singh [107] pointed out that a factor that contributes to the instability of bcc Co is its high electronic density of states at the Fermi energy. It was found [108] that at low temperatures the leading term in the electronic entropy is proportional to $N(E_F)$. Thus, a high $N(E_F)$ existing for a particular structure would very probably raise the so called 'band-energy' to a high value thus producing a maximum at the energy surface. In an approximation, the band energy which can be defined as the sum of the valence band eigenvalues up to the Fermi energy [109], is the leading term [109] in the total energy of a crystal in the sense that it determines the phase stability of many transition metals [109, 110]. In the following we will estimate the stability of the crystal phases of transition metals analysed in this work on the basis of their band structures alone.

It is possible for a material to become unstable with respect to vibrational modes before it becomes elastically unstable [111]. In some respects an elastic instability can

be thought of as a phonon instability with a vanishing wave vector [111]. Dynamical stability can be estimated by looking at the phonon dispersion relations; a large electronic density of states at the Fermi level often induces rich structure in the phonon dispersion relation curves [112]. In particular, transition metals possess unusual structural properties, which have their origin in the dominant influence of d valence band electrons on their electronic structure. They often exhibit pronounced phonon anomalies as a result of complex Fermi-surface geometries in conjunction with a strong electron-phonon coupling [99–105,113].

An anomaly in the phonon dispersion relation is manifested by a changed slope (i.e. a strongly damped or even negative slope) of the phonon dispersion curve. A damped slope produces 'soft-phonon modes' which signify incipient lattice instability [108,112,114,116–129]. More importantly, a negative slope in the phonon dispersion curves can, in addition, lead to 'negative' phonon frequencies making the lattice spontaneously unstable because stability requires the energy of phonons to be positive for all the wave vectors in the Brillouin zone. A phonon that lowers the energy of the crystal will grow in amplitude until the structure is driven to a new stable state [111]. Such phonons can produce displacements necessary for a martensitic phase transition [130].

Phonon anomalies in connection to martensitic transformations have been the topic of numerous experimental and theoretical studies [108,112,114,117–129,151–158]. It has been known for a long time now that phonon anomalies can be predicted from the band structure alone [114]. It is commonly believed that the origin of these anomalies lies in the coupling of lattice vibrations to electronic states near the Fermi energy [115,118]. Early investigations [112,113,118,126,128] explained the appearance of phonon anomalies as a Kohn effect, which consists in a strong coupling to electronic transitions between two almost parallel flat pieces of the Fermi surface and leads to the nesting condition:

$$\mathbf{q} + \mathbf{G} = \mathbf{k}' - \mathbf{k} \tag{2}$$

where $\mathbf{q}$ is the phonon wave vector, $\mathbf{k}'$, $\mathbf{k}$ lie on the Fermi surface, and $\mathbf{G}$ is a reciprocal lattice vector of the analysed crystal structure. It was shown that even less spectacular broad and shallow anomalies observed in phonon spectra can be traced back to a number of nesting vectors ($\mathbf{q}+\mathbf{G} = \mathbf{k}' - \mathbf{k}$) which cluster in a certain region of the Brillouin zone [126]. Now, let us see how these considerations can be applied to bcc Rh, which possesses a very high DOS at the Fermi-energy.

7.2 The instability of bcc Rh

To be stable, a crystal has to satisfy some stability criteria. For a cubic crystal the three stability criteria are:

$$C_{11} + 2C_{12} > 0, \qquad C_{44} > 0, \qquad C_{11} - C_{12} > 0 \tag{3}$$

where C_{ij} are the elastic constants [185]. The first relation corresponds to the bulk modulus $B = (C_{11} + 2C_{12})/3$ and the second and third one to shear constants [185]. The elastic constants C_{44} and $C_{11} - C_{12}$ are the trigonal and tetragonal shear moduli $C' = (C_{11} - C_{12})/2$, respectively. The former gives the stability (or instability) of a cubic crystal against a trigonal distortion. In a trigonal phase transformation the cubic lattice is expanded or contracted in the $\langle 111\rangle$-direction in such a way that: (i) the atomic volume remains constant and (ii) the six-fold symmetry of the $\{111\}$) direction is preserved during the transformation [168,172,175]. A bcc lattice can be in this way transformed into a fcc one, and vice-versa. The tetragonal shear modulus determines the ability of a system to resist a phase transformation by tetragonal distortions, during which the cubic lattice is expanded in the $\langle 100\rangle$ direction with the atomic volume remaining constant. Let us see now how the trigonal and tetragonal shear moduli can be predicted for bcc Rh on the grounds of the band structure alone.

In the preceding section we have shown that the dominant contribution to the electronic density of states at the Fermi energy comes for bcc Rh from flat bands positioned around symmetry points P of the bcc BZ, in particular along the P-N line. Let us see now how the crystal phase stability of the hypothetical bcc structure of Rh can be determined on the grounds of the topology of its Fermi surface. Figure 7 shows the distribution of the P-N lines in the momentum space. They constitute the cube marked with dashed lines in Figure 7b. We observe that there are many directions in which nesting vectors exist which connect P-N lines and, in this way, parallel flat pieces of the Fermi surface. Two of them: $\langle 100\rangle_{\rm bcc}$ and $\langle 110\rangle_{\rm bcc}$ deserve special attention since they are high symmetry directions.

7.2.1 Fermi-surface in the $\langle 100\rangle_{\rm bcc}$-direction

In the $\langle 100\rangle_{\rm bcc}$ direction the periodicity along the PN lines of the bcc bulk BZ is half the periodicity of the BZ in that direction (see Fig. 7b). Hence, in that direction the wave vectors **k'**–**k** connecting flat pieces of the Fermi surface (situated along the PN-lines of the bcc BZ) are equal to half the reciprocal lattice vectors in the $\langle 100\rangle_{\rm bcc}$ direction:

$$(\mathbf{k}' - \mathbf{k})_{bcc}^{\langle 100\rangle} \quad = \quad \frac{1}{2}\mathbf{G}_{bcc}^{\langle 100\rangle}. \tag{4}$$

Consequently, it follows from equation (2) that:

$$\mathbf{q}_{\mathbf{bcc}}^{\langle \mathbf{100}\rangle} + \mathbf{G}_{bcc}^{\langle 100\rangle} \quad = \quad \frac{1}{2}\mathbf{G}_{bcc}^{\langle 100\rangle}, \tag{5}$$

which further implies:

$$\mid \mathbf{q}_{\mathbf{bcc}}^{\langle \mathbf{100}\rangle} \mid \quad = \quad \frac{1}{2} \mid \mathbf{G}_{bcc}^{\langle 100\rangle} \mid \quad = \quad (k_{bcc}^{\langle 100\rangle})_{BZ}. \tag{6}$$

So, the topology of the Fermi surface of bcc Rh indicates the existence of an anomaly in the phonon dispersion curve in the $\langle 100\rangle_{\rm bcc}$ direction (ΓH direction of the bcc bulk BZ) at the zone boundary ($(k_{\rm bcc}^{\langle 100\rangle})_{\rm BZ}$). This means that there should exists an anomaly in the phonon

branch in the ΓH direction at the BZ boundary. The long-wave mode of this branch corresponds to C_{44} [127], with the related shear constant being the slope of the respective phonon-branch at $\mathbf{q} \to 0$. Since the topology of the Fermi surface indicates the existence of an anomaly in the phonon branch in the $\langle 100 \rangle_{\mathrm{bcc}}$-direction at the zone boundary (H) and not at the origin (Γ), the trigonal shear modulus C_{44} should be finite and positive. Consequently, the lattice structure of bcc Rh should be stable against trigonal deformations. This is also to be expected from crystallographic considerations: along the trigonal transformation path from bcc to fcc or from fcc to bcc the lattice passes through a simple cubic structure. In such a structure each atom lies on-top of the next-nearest neighbours of the adjacent lattice planes. This raises the total energy of the system, thus creating a high energy barrier along the trigonal transformation path between the bcc and fcc lattice [168,172,175]. In the following section two transformation paths will be discussed which transform the bcc lattice into close-packed ones (fcc or hcp) without passing through an energy barrier.

7.2.2 Fermi surface in the $\langle 110 \rangle_{\mathrm{bcc}}$ direction

The situation in the $\langle 110 \rangle_{\mathrm{bcc}}$ direction is different than that in the $\langle 100 \rangle_{\mathrm{bcc}}$-direction. The difference consists in the fact that only in the former direction the periodicity of the PN lines of the bcc bulk BZ is equal to the periodicity of the BZ in that direction (see Figs. 7b, c). Hence, only in the $\langle 110 \rangle_{\mathrm{bcc}}$ direction the nesting vector is almost equal to the reciprocal lattice vector in the respective direction. By way of explanation, there exists a cluster of nesting vectors in the $\langle 110 \rangle_{\mathrm{bcc}}$ direction with the property:

$$(\mathbf{k}' - \mathbf{k})_{bcc}^{\langle 110 \rangle} \simeq \mathbf{G}_{bcc}^{\langle 110 \rangle}. \tag{7}$$

It follows from equation (2) that:

$$\mathbf{q}_{bcc}^{\langle 110 \rangle} + \mathbf{G}_{bcc}^{\langle 110 \rangle} \simeq \mathbf{G}_{bcc}^{\langle 110 \rangle}, \tag{8}$$

and further:

$$\mathbf{q}_{bcc}^{\langle 110 \rangle} \to 0. \tag{9}$$

Consequently, the phonon branch in the $\langle 110 \rangle_{\mathrm{bcc}}$ direction should have an anomaly already at $\mathbf{q} \to 0$. This anomaly implies a negative value of the related shear constant. The shear constant related to the phonon branch in the $\langle 110 \rangle_{\mathrm{bcc}}$ direction is the tetragonal shear modulus $C' = (C_{11} - C_{12})/2$ [127]. So, the existence of the Kohn anomaly for bcc Rh in the $\langle 110 \rangle_{\mathrm{bcc}}$ direction at $\mathbf{q} \to 0$ suggests that the tetragonal shear modulus $C' = (C_{11} - C_{12})/2$ is unstable (e.g. negative). Indeed, many calculations have shown that the shear elastic constant C' is negative for the bcc structures [183] of native fcc or hcp metals [66, 67, 107, 159–177]. Moreover, there are no energy barriers to prevent the bcc phase of native fcc and hcp metals from a lattice distortion toward the fcc or hcp structure, the bcc phase being related to a maximum (or at least to a saddle point) of the energy surface [159, 171, 177]. The trend displayed by the energy difference between the fcc and bcc crystal structures has been found to be similar to that of the tetragonal shear constant [109, 161]. Calculations of the phonon dispersion curves have shown that, indeed, for structures with a negative tetragonal elastic constant C' the corresponding dispersion is imaginary [127]. In addition, it was found for metals with native close-packed phases that the entire $T_1(\xi, \xi, 0)$ mode of the bcc structure with the polarisation along $[1\bar{1}0]$ is unstable. The zone boundary mode of this branch $T_{[1\bar{1}0]}(\frac{1}{2}, \frac{1}{2}, 0)$ lies for these systems at the highest 'negative' frequencies. This phonon was studied in several systems [105, 108, 112, 119, 121–123, 127, 128, 178–181] since $T_{[1\bar{1}0]}(\frac{1}{2}, \frac{1}{2}, 0)$ together with a tetragonal shear constant transform the bcc structure into the hcp one. The negative bcc $T_{[1\bar{1}0]}(\xi, \xi, 0)$ branch strongly lowers the free energy along this transition path and obviously makes the hcp minima fall below the bcc free energy [119]. We will now briefly analyse the transformation path from the bcc structure into a close-packed one (fcc or hcp).

7.3 The bcc to fcc tetragonal phase transformation path

A negative shear modulus C' makes the bcc lattice unstable against a tetragonal transformation into the fcc lattice. Along this transformation path, also known as the Bain transformation path, the cubic lattice is continuously expanded (bcc to fcc transformation) or contracted (fcc to bcc transformation) in the $\langle 001 \rangle$ direction, since the volume per atom is kept fixed (see for example Paidar et al. [182]). All intermediate structures encountered along this path are tetragonal with the $\{001\}$ lattice plane as the basis. Consequently, a (001)-oriented bcc film will transform into a (001)-oriented fcc one. The difference between the two orientations is that the fcc(001) lattice plane is much more densely packed than the bcc(001) atomic plane. Here lies the reason why a pseudomorphic film grown (in a phase modification [16]) on (001)-oriented cubic substrates very often does not transform into its native (001)-oriented fcc or bcc phase: due to large differences between the inter-atomic distances in the fcc(001) and bcc(001) planes, the native (001) atomic plane has a very bad fit to the (001)-oriented substrate in the case when the ps-film is in a crystal phase modification (bcc for native fcc metals, or fcc for native bcc metals). The epitaxial constraint imposed by the (001)-oriented substrate on the growing film prevents the film from adopting the (001)-oriented native cubic phase. As a result, the film finds another way of transforming its pseudomorphic structure into the native one. An example of such a transformation is provided by the growth of Fe (whose ground phase is bcc) on Cu(001). After some 5 to 10 pseudomorphic layers (i.e. with a fct(001) film structure) of Fe have grown, the film structure transforms into the (011)-oriented bcc phase [19] and not into the bcc(001) one. Now, the bcc structural modification of films with the native close-packed (fcc or hcp) phase (e.g. Rh and Pd) can be obtained by pseudomorphic growth on

suitable (001)-oriented substrates [27]. Similarly to Fe on Cu(001), pseudomorphic bcc(001)-oriented films [16] do not transforms into the native fcc(001) phase via the Bain transformation path either: instead they transform into a (011)-oriented close-packed structure. However, the difference to the case of Fe is that the native phase of metals like Rh and Pd is fcc. The fcc(011)-film orientation drastically differs from the bcc(011)-film one. In the bcc(011) orientation the densest-packed atomic planes (which are the bcc(011) planes) of a film lie parallel to the surface, whereas in the case of a close-packed (011)-film orientation they are the close-packed planes (which are (111) for the fcc structure and the (0001) for the hcp structure, respectively). The film lattice transformation from the pseudomorphic bcc(001) orientation into the (011) orientation of the close-packed phase –which is hcp and not fcc– drastically reduces the thickness limit of the pseudomorphic bcc-phase, as will be shown below.

7.4 The bcc to hcp hexagonal phase transformation path

There exists a crystal structure transformation path which transforms the (001)-oriented bcc phase into a close-packed one with only a minor change of the atomic density in the atomic planes parallel to the substrate surface. This transformation path is called the hexagonal path. It connects the bcc and the close-packed lattices (e.g. fcc and hcp). The transformation is a combination of an homogeneous deformation that preserves the atomic volume, with the shuffling of (e.g. alternate) close packed atomic planes (bct(110), fcc(111) or hcp(0001)) in (e.g. opposite) directions [175,182]. Starting with the bcc phase, the homogeneous part of the transformation is a small contraction of the bcc lattice in the [001] direction by holding the atomic volume constant. Upon such a transformation the bcc(110) planes contract into hexagonal close-packed ones (hcp(0001) or fcc(111)). Finally, sliding these atomic planes in the $[1\bar{1}0]_{\rm bcc}$ direction transforms the lattice into an hcp or fcc one. As an example, a (001)-oriented bcc (or bct) film (e.g. a pseudomorphic film) transforms into a (110)-oriented fcc or hcp ($(11\bar{2}0)$) one. If the (001)-oriented bcc (or bct) film is grown on a (001)-oriented cubic substrate, the transformation of the film-structure to the (110)-oriented fcc one has to surpass an energy barrier. In the case when the deposited film transforms to the hcp(110) structure the total energy continuously decreases until it becomes equal to that of the hcp structure.

We can therefore conclude that:

1. the existence of an energy barrier in the bcc(001)–fcc(110) transformation in substrate-supported films with native close-packed phases [186]
2. the absence of an energy barrier in the bcc(001)–hcp(110) and in the bcc(001)–dhcp(110) film transformation [175,186]
3. the existence of an energy barrier in the fcc–hcp and in the fcc–dhcp transformation path [186,189]

are the main reasons why films with the native fcc phase grow in the hexagonal $(11\bar{2}0)$ orientation on suitable substrates over a large thickness (over 100 MLs) without transforming back into the native fcc phase even when the films are stripped off their substrates [27,186–188]. The orientation relationship between hcp and dhcp films and (001)-oriented (e.g. bcc) substrates is: $(11\bar{2}0)[0001]_{film} \parallel (001)[110]_{substrate}$ (see the Figs. 5 and 6 in Hüger and Osuch [33]). The four-fold symmetry of the (001)-oriented substrate surface induces two sets of orthogonal $(11\bar{2}0)$-oriented film domains. In contrast to the (001) substrate surface, which has four-fold symmetry, the $(11\bar{2}0)_{film}$ surface has only two-fold symmetry. Although the orthogonal [110]- and $[1\bar{1}0]$-directions of the (001) substrate surface are equivalent, the orthogonal directions $[0001]_{film}$ and $[1\bar{1}00]_{film}$ are not. Therefore, those films grow on bcc(001) substrates in two orthogonal domains with rectangular shapes [27,194,195]– one with $[0001]_{film} \parallel [011]_{bcc}$ and $[1\bar{1}00]_{film} \parallel [0\bar{1}1]_{bcc}$ and the other with $[0001]_{film} \parallel [0\bar{1}1]_{bcc}$ and $[1\bar{1}00]_{film} \parallel [011]_{bcc}$ [27,28]. This domain topology is maintained in films stripped off the substrates and is the main cause of the stability of the hcp and dhcp phase in the stripped films [186].

7.5 Enlarging the thickness of Rh films with the bcc crystal structure

We notice that the [001]-direction of a ps-film grown on (001)-oriented cubic substrates lies perpendicularly to the film surface and thus along the direction where the substrate has the smallest influence on the film structure. This allows the film to relax its crystal structure in the surface normal direction by performing small shears required to transform the dense-packed bct(110)-planes (which stay perpendicular to the film surface) into close-packed ones ((111) for a fcc-stacking sequence or (0001) for an hexagonal-stacking sequence). Once the close-packed planes are formed (perpendicularly to the surface) they automatically slide from the bct stacking sequence (the so-called unstable stacking sequence [135,136,191–193]) into the hexagonal one [186]. Atomic simulations have shown that this transformation into an hcp-stacking sequence (and not into a fcc-stacking sequence [172,184,185]) cannot be prevented, not even by the existence of a substrate [172]. Thus, in contrast to the growth of films with the native fcc phase in the $(11\bar{2}0)$-oriented hcp structure, the growth of such films in the bcc structure is restricted to only first few monolayers (up to 2 or 9 monolayers) [27,186]. This critical thickness of the pseudomorphic growth can be enlarged by suitable surfactants [18,24,196,198–201] which block the shift of ps bct(110) planes into hcp positions [196] or by imposing a suitable epitaxial constraint on the both interfaces in multilayers [35,184,196,197,202–209]. The suppression of the hcp$(11\bar{2}0)$ growth also occurs in the presence of oxygen. Kim et al. [24] have demonstrated that a submonolayer coverage of oxygen can double the ps-range of Co deposited on Fe(001). Later studies [200,201] confirmed this result by finding that the presence of oxygen causes

a delayed onset of the bct-hcp transition. Very likely oxygen impedes the shift of the compressed bct(110) planes (the hexagons) into hcp positions thereby preserving the pseudomorphic phase. This phase can also be enlarged by the effect of two suitable interfaces in superlattices [35, 184, 196, 197, 202–209]. In the case of Rh, the growth of Rh films in Rh/V(001) superlattices would be a suitable way of obtaining thicker (e.g. at least 10 ML thick) bcc (or bct) Rh films by ps growth. Of course, the development of the $(11\bar{2}0)$-oriented hexagonal structure (after the ps-growth) is a serious limitation to achieving relatively thick bcc (or bct) Rh films on suitable substrates. The effect of a surfactant (e.g. oxygen [24,200,201] or of alumina [196, 202, 203] (Al_2O_3)) on the stability and thickness of these films could be an interesting topic of a further study of this epitaxial system.

Summarising:
(i) the instability of the bcc structure for metals with close-packed native phases implies the difficulty of growing thick films in the bcc phase modification,
whereas
(ii) the metastability of the hcp structure in metals with the native fcc phase and the special epitaxial relationship of $(11\bar{2}0)$-oriented hcp films grown on (001)-oriented cubic substrates are responsible for the stability of the hcp phase in thick (i.e. over 100 monolayers thick) films even when the films are stripped off their substrates.

8 Conclusions

First principles self-consistent DFT calculations with spin-orbit coupling included show that the driving force behind the induction of ferromagnetic order at the equilibrium lattice constant in bulk Rh and Pd is crystal symmetry change. The change of symmetry from fcc to bcc for Rh and from fcc to hcp/dhcp for Pd induces ferromagnetism in bulk Rh and Pd at the optimum lattice constants with the magnetic moments of 0.26 μ_B, 0.16 μ_B, 0.11 μ_B per atom for bcc Rh, hcp Pd and dhcp Pd, respectively. Due to the spin-orbit interaction, the spin anisotropies induce small orbital moments of 0.06 μ_B, 0.07 μ_B, 0.05 μ_B per atom for bcc Rh, hcp Pd and dhcp Pd, respectively. They enlarge the total magnetic moments to 0.32 μ_B, 0.23 μ_B, 0.16 μ_B per atom for bcc Rh, hcp Pd and dhcp Pd, respectively. The appearance of ferromagnetic order in bcc Rh and hcp/dhcp Pd is strongly related to the position of the Fermi level at the top of the strongest peak of the bcc- and hcp/dhcp-induced DOS, respectively. Flat bands lying at the surface of the respective Brillouin zones were found to be at the origin of these peaks.

The origin of these flat bands was found to be the translation symmetry of the bcc lattice which makes the Bloch states with symmetry e_g narrow along the $\Gamma - N - P - \Gamma$ line of the bcc BZ. This happens because the magnitude of the wave function between atoms does not change significantly with varying k-vectors of this k-line. As a consequence, the energy does not change significantly along this line either because k-vectors on this line are not aligned with the $\langle 100 \rangle$ directions into which orbitals e_g point. In addition, the high abundance of symmetry points on the N-P line and its alignment with the direction of the weakest bonds ($\langle 100 \rangle$) in a bcc transition metal makes the band with symmetry e_g flat along this line. This flat band induces a strong sharp peak in the bcc DOS. The d-band occupancy of Rh locates the Fermi level exactly at the top of this sharp peak inducing ferromagnetic order in bcc Rh at the optimum lattice constant.

The strongest DOS peak situated at the top of the valence band induced by the hcp or dhcp crystal structure of a d-band metal is caused by flat bands which lie at the surface of the hcp BZ. These flat bands are along k-lines aligned with the [0001] direction where (i) in momentum space there exists a high abundance of symmetry points (the M-L-line) and (ii) in the real space the bonds between atoms are the weakest. The latter happens because the stacking sequence direction (the [0001] direction) is the most remote direction from the close-packed hexagonal atomic planes (0001) of the close-packed structure. The d-band occupancy of Pd places the Fermi energy at the top of the strongest peak induced by the hcp/dhcp structure. This makes the DOS at the Fermi energy high enough to induce ferromagnetic order in hcp/dhcp Pd at the optimum lattice constant.

We have shown on the grounds of the electronic structure alone– in particular on the grounds of the structure of the Fermi surface– that the bcc crystal structure of Rh is stable along a trigonal transformation path, but unstable along a tetragonal or hexagonal one. We pointed out that, in general, the metastable nature of the hexagonal (hcp/dhcp) structure of metals with the native fcc phase (e.g. Rh and Pd) and the special epitaxial relationship of $(11\bar{2}0)$-oriented films grown on (001)-oriented cubic substrates (e.g. Rh and Pd on W(001)) lead to the stability of the hexagonal structure in thick films even when they are stripped off their substrates. In contrast, the bcc and bct phase modifications of metals with the native close-packed structure are not metastable and hence they can not form free standing films. Even the epitaxial constraint of a suitable substrate can not stabilise them over a large film thickness.

One of us (KO) would like to thankfully acknowledge the financial assistance received from the Polish State Committee for Scientific Research through the research grant PBZ/KBN/044/P03/2001.

References

1. E.C. Stoner, Proc. Roy. Soc. A **165**, 372 (1938); Proc. Roy. Soc. A **169**, 339 (1939)
2. L. Fritsche, B. Weimert, Phys. Stat. Sol. (b) **208**, 287 (1998)
3. L. Fritsche, private communication; L. Fritsche, J. Koller, J. Solid State Chem. **176**, 652 (2003)
4. J. Kübler, *Theory of Itinerant electron Magnetism* (Oxford Science Publications, 2000), ISBN 0198500289
5. D.J. Singh, in *Electronic Structure and Magnetism of Complex Materials* edited by D.J. Singh, D.A.

Papaconstantopoulos (Springer, Berlin, Heidelberg, New York, 2003), ISBN 3540433821
6. A. Delin, E. Tossatti, R. Weht, Phys. Rev. Lett. **92**, 057201 (2004)
7. A. Delin, E. Tossatti, arxiv.org/abs/cond-mat/04011559
8. A. Delin, E. Tossatti, Phys. Rev. B **68**, 144434 (2003)
9. A. Delin, E. Tossatti, Surf. Sci. **566-568**, 262 (2004)
10. V.S. Stepanyuk, P. Bruno, A.L. Klavysyuk, A.N. Baranov, W. Hergert, I. Mertig, contribution O 33.3 to the Spring Meeting 2003 of the German, Netherland, Austrian and Czech physical society. Abstract written in English available at http://www.dpg-tagungen.de/prog/html/O_33.html
11. L. Fritsche, J. Noffke, H. Eckardt, J. Phys. F: Met. Phys. **17**, 943 (1987)
12. V.L. Moruzzi, P.M. Marcus, Phys. Rev. B **39**, 471 (1989); V.L. Moruzzi, P.M. Marcus, Phys. Rev. B **42**, 10322 (1990)
13. Ming J. Zhu, D.M. Bylander, L. Kleinman, Phys. Rev. B **42**, 2874 (1990)
14. S. Blügel, Phys. Rev. Lett. **39**, 851 (1992)
15. The deposition of metals on suitable substrates can, via pseudomorphism [17], enlarge the in-plane lattice constant of the film. This does not lead, however, to an enlarged atomic volume, because in the direction perpendicular to the surface, the film relaxes, reducing its out-of-plane lattice constant in such a way, that the atomic volume is preserved (equal to that of the natural phase)
16. Pseudomorphic growth [17] is a convenient route to growing films in a crystal phase modification. The so called fcc(100) and bcc(100) structures are stabilised via pseudomorphic growth [17], where the lateral periodicity of the film is the same as that of the (100)-oriented metallic substrate surface. Due to the conservation of the atomic volume the film relaxes its out-of-plane interatomic distances by tetragonal deformation, forming a bct(100)- or a fct(100)-oriented film
17. F. Jona, P.M. Marcus, Surf. Rev. Lett. **4**, 817 (1997)
18. A. Kirilyuk, J. Giergiel, J. Shen, J. Kirschner, Phys. Rev. B **52**, R11672 (1995)
19. J. Shen, H. Jenniches, Ch. V. Mohan, J. Barthel, M. Klaua, P. Ohresser, J. Kirschner, Europhys. Lett. **43**, 349 (1998)
20. M.T. Kief, W.F. Egelhoff, Jr., Phys. Rev. B **47**, 10785 (1993), and references therein
21. G.R. Harp, R.F.C. Farrow, D. Weller, T.A. Rabedeau, R.F. Marks, Phys. Rev. B **48**, 17538 (1993)
22. J. Fassbender, G. Güntherodt, C. Mathieu, B. Hillebrands, R. Jungblut, J. Kohlhepp, M.T. Johnson, D.J. Roberts, G.A. Gehring, Phys. Rev. B **57**, 5870 (1998)
23. S.K. Kim, F. Jona, P.M. Marcus, J. Phys.: Condens. Matter **8**, 25 (1996)
24. S.K. Kim, C. Petersen, F. Jona, P.M. Marcus, Phys. Rev. B **54**, 2184 (1996)
25. H. Wieldraaijer, J.T. Kohlhepp, P. LeClair, K. Ha, W.J.M. de Jonge, Phys. Rev. B **67**, 224430 (2003), and references therein
26. H. Wormeester, E. Hüger, E. Bauer, Phys. Rev. B **57**, 10120 (1998)
27. E. Hueger, H. Wormeester, E. Bauer, Surf. Sci. **438**, 185 (1999)
28. H. Wormeester, E. Hüger, E. Bauer, Phys. Rev. Lett. **81**, 854 (1998); **77**, 1540 (1996)
29. E. Hüger, K. Osuch, Europhys. Lett. **62**, 278 (2003)
30. E. Hüger, K. Osuch, Solid State Commun. **132**, 97 (2004)
31. E. Hüger, K. Osuch, Europhys. Lett. **63**, 90 (2003)
32. E. Hüger, K. Osuch, Eur. Phys. J. B **37**, 149 (2004)
33. E. Hüger, K. Osuch, J. Electron Spectrosc. Rel. Phenom. **141**, 13 (2004)
34. F. Jona, X.Z. Ji, P.M. Marcus, Phys. Rev. B **68**, 075421 (2003)
35. P. Bayle-Guillemaud, J. Thibault, Phil. Mag. A **77**, 475 (1998)
36. M.C. Saint-Lager, M. Brunel, D. Raoux, M. Piecuch, J. Magn. Magn. Mater. **148**, 9 (1995)
37. S.A. Dregia, R. Banerjee, H.L. Fraser, Scripta Mater. **29**, 217 (1998)
38. R. Banerjee, S.A. Dregia, H.L. Fraser, Acta Mater. **47**, 4225 (1999)
39. G.B. Thompson, R. Banerjee, S.A. Dregia, H.L. Fraser, Acta Mater. **51**, 5285 (2003)
40. G.B. Thompson, R. Banerjee, H.L. Fraser, Appl. Phys. Lett. **83**, 3471 (2003)
41. G.B. Thompson, R. Banerjee, H.L. Fraser, Appl. Phys. Lett. **84**, 1082 (2004)
42. A.J. Melmed, V. Maurice, O. Frank, J.H. Block, J. Cryst. Growth **84**, 123 (1987)
43. S. Illy, O. Tillement, F. Macizaud, J.M. Dubois, F. Massicot, Y. Fort, J. Ghanbaja, Phil. Mag. A **79**, 1021 (1999)
44. A.J. Cox, J.G. Louderback, L.A. Bloomfield, Phys. Rev. Lett. **71**, 923 (1993)
45. A.J. Cox, J.G. Louderback, S.E. Apsel, L.A. Bloomfield, Phys. Rev. B **49**, 12295 (1994)
46. T. Taniyama, E. Ohta, T. Sato, Europhys. Lett. **38**, 195 (1997)
47. L. Vitos, B. Johansson, J. Kollár, Phys. Rev. B **62**, R11957 (2000)
48. B.V. Reddy, S.N. Khanna, B.I. Dunlap, Phys. Rev. Lett. **70**, 3323 (1993)
49. B. Sampedro, P. Crespo, A. Hernando, R. Litrán, J.C. Sánchez López, C. López Carres, A. Fernandez, J. Ramírez, J. González Calber, M. Valler, Phys. Rev. Lett. **91**, 237203 (2003)
50. K. Saroj, S.E. Najak, P. Weber, K. Jena Wildberger, R. Zeller, P.H. Dederichs, V.S. Stepanyuk, W. Hergert, Phys. Rev. B **56**, 8849 (1997)
51. I. Morrison, D.M. Bylander, L. Kleinman, Phys. Rev. Lett. **71**, 1083 (1993)
52. S.C. Wu, K. Garrison, A.M. Begley, F. Jona, P.D. Johnson, Phys. Rev. B **49**, 14081 (1994)
53. P. Hohenberg, W. Kohn, Phys. Rev. **136**, B864 (1964)
54. W. Kohn, L.J. Sham, Phys. Rev. **140**, A1133 (1964)
55. P. Blaha, K. Schwarz, G.K.H. Madsen, D. Kvasnicka, J. Luitz, WIEN2k, An Augmented Plane Wave + Local Orbitals Program for Calculating Crystal Properties (Karlheinz Schwarz, Technische Universität Wien, Austria), 2001 ISBN 3-9501031-1-2
56. M. van Schilfgaarde, V.P. Antropov, B.N. Harmon, J. Appl. Phys. **79**, 4799 (1996)
57. M. Körling, J. Häglund, Phys. Rev. B **45**, 13293 (1992)
58. V. Ozolins, M. Körling, Phys. Rev. B **48**, 18304 (1993)

59. It is well known that magnetic electronic structure calculations based on the LDA approximation to the exchange-correlation potential predict a wrong ground state for Fe (fcc instead of bcc). This problem has been solved by the introduction of gradient corrections to the LDA. (For a list of references on this subject see P. Söderlind et al. [60,61])
60. P. Söderlind, R. Ahuja, O. Eriksson, J.M. Willis, B. Johansson, Phys. Rev. B **50**, 5918 (1994)
61. P. Söderlind, J.A. Moriaty, J.M. Willis, Phys. Rev. B **53**, 14063 (1996)
62. The reason why the LSDA and not the more modern GGA approximation was used in this study is that the former gives better results for heavier elements whereas the latter is more suitable for lighter ones [63]. This is further confirmed by our spin-polarised GGA calculation of the magnetic moment of Pd in the fcc phase at the optimum lattice constant. It produces a non-vanishing magnetic moment per atom, leading to the conclusion that fcc Pd is ferromagnetically ordered, in contradiction to experimental observations
63. P. Blaha, private communication
64. V.L. Moruzzi, P.M. Marcus, P.C. Pattnaik, Phys. Rev. B **37**, 8003 (1988)
65. J. Goniakowski, M. Podgorny, Phys. Rev. B **44**, 12348 (1991); G. Cort, R.D. Taylor, J.O. Willis, J. Appl. Phys. **53**, 2064 (1982)
66. H.C. Herper, E. Hoffmann, P. Entel, Phys. Rev. B **60**, 3839 (1999)
67. S. Fox, H.J.F. Jansen, Phys. Rev. B **60**, 4397 (1999)
68. V.L. Moruzzi, P.M. Marcus, K. Schwarz, P. Mohn, Phys. Rev. B **34**, 1784 (1986); V.L. Moruzzi, Phys. Rev. Lett. **57**, 2211 (1986)
69. N.B. Brookes, A. Clarke, P.D. Johnson, Phys. Rev. B **46**, 237 (1992), and references therein
70. Changfeng Chen, Phys. Rev. B **43**, 6347 (1991)
71. For a list of articles see the home-page of the Wien2k calculation package (`http://www.wien2k.at`)
72. T. Noboru, C.T. Chan, K.M. Ho, Phys. Rev. B **40**, 1565 (1989)
73. H.L. Skriver, Phys. Rev. B **31**, 1909 (1985)
74. C.S. Yoo, H. Cynn, P. Söderlind, V. Iota, Phys. Rev. Lett. **84**, 4132 (2000)
75. N. Boernsen, B. Mayer, O. Grotheer, M. Fähnle, J. Phys.: Condens. Matter **11**, L287 (1999)
76. C. Celinski, B. Heinrich, J.F. Cochran, W.B. Muir, A.S. Arrot, J. Kirschner, Phys. Rev. Lett. **65**, 1156 (1990)
77. E.E. Fullerton, D. Stoeffler, K. Ounadjela, B. Heinrich, Z. Celinski, J.A.C. Bland, Phys. Rev. B **51**, 6364 (1995)
78. A.E. Garcia, V. Gonzáles-Robles, R. Baquero, Phys. Rev. B **59**, 9392 (1999)
79. M.A. Tomaz, D.C. Ingram, G.R. Harp, D. Lederman, E. Mayo, W.L. O'Brien, Phys. Rev. B **56**, 5474 (1997)
80. Self-consistent DFT calculations carried out without spin-orbit coupling give larger magnetic moments than those in which spin-orbit coupling is included, e.g. they give the magnetic moment of 0.34 μ_B (instead of 0.16 μ_B) for hcp Pd
81. For an illustration of how a tetragonal deformation transforms fcc into bcc (and vice-versa) see Figure 1 in Kraft et al. [82]
82. T. Kraft, P.M. Marcus, M. Methfessel, M. Scheffler, Phys. Rev. B **48**, 5886 (1993)
83. Sticht, J. Kübler, Solid State Comm. **53**, 529 (1985)
84. H. Ebert, R. Zeller, B. Drittler, P.H. Dederichs, J. Appl. Phys. **67**, 4576 (1990)
85. I. Cabria, B. Nonas, R. Zeller, P.H. Dederichs, Phys. Rev. B **65**, 054414 (2002)
86. M. Yasui, Physica B **149**, 139 (1988)
87. A.R. Mackintosh, O.K. Andersen, in *Electrons at the Fermi Surface*, edited by M. Springford (Cambridge University Press, Cambridge, 1980), Chap. *The Electronic Structure of Transition Metals*
88. O.K. Andersen, Solid State Commun. **13**, 133 (1973)
89. D.G. Pettifor, J. Phys. C **3**, 367 (1970)
90. C.J. Bradley, A.P. Cracknell, *The Mathematical Theory of Symmetry in Solids* (Clarendon Press, Oxford, 1972)
91. S. Deng, A. Simon, J. Köhler, J. Solid State Chemistry **176**, 412 (2003)
92. L. Fritsche, private communication
93. S.L. Altmann, *Band Theory of Metals* (Pergamon Press, Oxford, New York, 1970)
94. F.J. Ohkawa, Phys. Rev. B **65**, 174424 (2002)
95. P. Blaha, K. Schwartz, P.H. Dederichs, Phys. Rev. B **38**, 9368 (1988)
96. J.X. Zheng-Johansson, O. Eriksson, B. Johansson, Phys. Rev. B **59**, 6131 (1999)
97. A.T. Paxton, M. Methfessel, M. Polatoglou, Phys. Rev. B **41**, 8127 (1990), and references therein
98. E. Hüger, K. Osuch, Thin Solid Films (submitted)
99. S. Deng, A. Simon, J. Köhler, J. Superconductivity **17**, 227 (2004)
100. S. Deng, A. Simon, J. Köhler, J. Superconductivity **16**, 477 (2003)
101. S. Deng, A. Simon, J. Köhler, J. Superconductivity **16**, 919 (2003)
102. S. Deng, A. Simon, J. Köhler, J. Superconductivity **15**, 635 (2002)
103. S. Deng, A. Simon, J. Köhler, J. Phys. Chem. Solids **62**, 1441 (2001)
104. S. Deng, A. Simon, J. Köhler, J. Am. Chem. Soc. **124**, 10712 (2002)
105. N. Suzuki, M. Otani, J. Phys.: Condens. Matter **14**, 10869 (2002)
106. W. Pepperhoff, M. Acet, *Konstitution und Magnetismus* (Springer, Berlin, 2000), p. 30
107. A.Y. Liu, D.J. Singh, Phys. Rev. B **47**, 8515 (1993)
108. A.Y. Liu, A.A. Quong, J.K. Freericks, E.J. Nicol, E.C. Jones, Phys. Rev. B **59**, 4028 (1999)
109. V.L. Sliwko, P. Mohn, K. Schwarz, P. Blaha, J. Phys.: Condens. Matter **8**, 799 (1996)
110. D.G. Pettifor, Acta Materialia **51**, 5649 (2003) *The Golden Jubilee Issue*, and references therein
111. D.M. Clatterbuck, C.R. Krenn, M.L. Cohen, J.W. Morris Jr., Phys. Rev. Lett. **91**, 135501 (2003)
112. C.M. Varma, W. Weber, Phys. Rev. B **19**, 6142 (1979)
113. R. Heid, L. Pintschovius, W. Reichardt, K.-P. Bohnen, Phys. Rev. B **61**, 12059 (2000)
114. C.M. Varma, W. Weber, Phys. Rev. Lett. **39**, 1094 (1977)
115. As phonons have much smaller energies than electrons, they can only influence electronic states close to the Fermi level [103]
116. W. Cochran, *The Dynamics of Atoms in Crystals* (Edward-Arnold, London, ISBN-0713124393, 1973)
117. K.-M. Ho, C.-L. Fu, B.N. Harmon, Phys. Rev. B **28**, 6687 (1983)

118. K.-M. Ho, C.-L. Fu, B.N. Harmon, Phys. Rev. B **29**, 1575 (1984)
119. Y.-Y. Ye, Y. Chen, K.-M. Ho, B.N. Harmon, P.A. Lindgard, Phys. Rev. Lett. **58**, 1769 (1987)
120. R.M. Wentzcovitch, M.L. Cohen, Phys. Rev. B **37**, 5571 (1988)
121. W. Petry, A. Heiming, J. Trampenau, M. Alba, C. Herzig, H.R. Schober, G. Vogl, Phys. Rev. B **43**, 10933 (1991)
122. A. Heiming, W. Petry, J. Trampenau, M. Alba, C. Herzig, H.R. Schober, G. Vogl, Phys. Rev. B **43**, 10948 (1991)
123. J. Trampenau, A. Heiming, W. Petry, M. Alba, C. Herzig, W. Miekeley, H.R. Schober, Phys. Rev. B **43**, 10963 (1991)
124. F. Güthoff, W. Petry, C. Strassis, A. Heiming, B. Hennion, C. Herzig, J. Trampenau, Phys. Rev. B **47**, 2563 (1993)
125. W. Petry, J. Trampenau, C. Herzig, Phys. Rev. B **48**, 881 (1993)
126. A. Eichler, K.-P. Bohnen, W. Reichardt, J. Hafner, Phys. Rev. B **57**, 324 (1998)
127. K. Persson, M. Ekman, V. Ozoliņš, Phys. Rev. B **61**, 11221 (2000)
128. Y. Wang, R. Ahuja, M.C. Qian, B. Johansson, J. Phys.: Condens. Matter **14**, L695 (2002)
129. S.V. Rudin, M.D. Jones, R.C. Albers, Phys. Rev. B **69**, 094117 (2004)
130. Martensitic transformations are diffusion-less solid-to-solid crystal phase transitions characterised by a rapid change of crystal structure observed in many materials, being the basis of numerous technological applications [109, 119, 120, 131–150, 157]
131. G.B. Olson, H. Hartman, J. Phys. Colloq. France **43**, C4-855 (1982)
132. R. Bruinsma, A. Zangwill, Phys. Rev. Lett. **55**, 214 (1985)
133. P.-A. Lindgard, O.G. Mauritsen, Phys. Rev. Lett. **57**, 2458 (1986)
134. C.S. Barrett, T.B. Massalski, *Structure of Metals* (Pergamon Press, Oxford, 1987)
135. V.P. Dmitriev, S.B. Rochal, Y.M. Gufan, P. Tóledano, Phys. Rev. Lett. **60**, 1958 (1988); V.P. Dmitriev, S.B. Rochal, Y.M. Gufan, P. Tóledano, **62**, 2495 (1989)
136. I. Folkins, M.B. Walker, Phys. Rev. Lett. **65**, 127 (1990)
137. R.M. Wentzcovitch, H. Krakauer, Phys. Rev. B **42**, 4563 (1990)
138. R.M. Wentzcovitch, P.K. Lam, Phys. Rev. B **44**, 9155 (1991)
139. G.B. Olson, W. Oven, *Martensite* (ASM International, Materials Park, 1992)
140. E.K.H. Salje, *Phase Transitions in Ferroelectrics and Co-elastic Crystals* (Cambridge Univ. Press, Cambridge, 1993)
141. R.D. James, M. Wuttig, Philos. Mag. A **77**, 1273 (1998)
142. K. Otsuka, C.M. Wayman, *Shape Memory Crystals* (Cambridge Univ. Press, Cambridge, 1998)
143. Y.C. Shu, K. Bhattacharya, Philos. Mag. B **81**, 2021 (2001)
144. P. Tóledano, G. Krexner, M. Prem, H.-P. Weber, D.P. Dmitriev, Phys. Rev. B **64**, 144104 (2001)
145. H.Th. Hesemann, *Thesis* (Max-Plank Institute für Metallforschung, Stuttgart, 2002)
146. M.H. Bocanegra-Bernal, S.D. De la Torre, J. Mater. Sci. **37**, 4947 (2002)
147. A. Sozinov, A.A. Likhachev, N. Lanska, K. Ullakko, Appl. Phys. Lett. **80**, 1746 (2002)
148. P.-G. de Gennes, K. Okumura, Europhys. Lett. **63**, 76 (2003)
149. D.R. Trinkle, R.G. Hennig, S.G. Srinivasan, D.M. Hatch, M.D. Jones, H.T. Stokes, R.C. Albers, J.W. Wilkins, Phys. Rev. Lett. **91**, 025701 (2003)
150. K. Bhattacharya, *Microstructure of Martensite* (Oxford Univ. Press, Oxford, 2003)
151. J.D. Axe, D.T. Keating, S.C. Moss, Phys. Rev. Lett. **35**, 530 (1975)
152. Y. Noda, Y. Yamada, S.M. Shapiro, Phys. Rev. B **40**, 5995 (1989)
153. B.L. Zhang, C.Z. Wang, K.M. Ho, D. Turner, Y.Y. Ye, Phys. Rev. Lett. **74**, 1375 (1995)
154. O. Dubos, W. Petry, J. Neuhaus, B. Hennion, Eur. Phys. J. B **3**, 447 (1998)
155. U. Pinsook, G.J. Ackland, Phys. Rev. B **59**, 13642 (1999)
156. M. Porta, T. Cástan, Phys. Rev. B **63**, 134104 (2001)
157. J.R. Morris, K.M. Ho, Phys. Rev. B **63**, 224116 (2001)
158. M. Sanati, A. Saxena, T. Lookman, Phys. Rev. B **64**, 092101 (2002)
159. M.J. Mehl, L.L. Boher, Phys. Rev. B **43**, 9498 (1991)
160. G.W. Fernando, J. Mei, R.E. Watson, M. Weinert, J.W. Davenport, Phys. Rev. B **47**, 13636 (1993)
161. P. Söderlind, J. Wills, O. Eriksson, Int. J. Mod. Phys. B **7**, 203 (1993)
162. P.J. Craievich, M. Weinert, J.M. Sanchez, R.E. Watson, Phys. Rev. Lett. **72**, 3076 (1994)
163. P.J. Craievich, J.M. Sanchez, R.E. Watson, M. Weinert, Phys. Rev. B **55**, 787 (1995)
164. S. Kim, F. Jona, P.M. Marcus, J. Phys.: Condens. Matter **8**, 25 (1996); P.M. Marcus, F. Jona, J. Phys.: Condens Matter **9**, 6241 (1997)
165. P. Alippi, P.M. Marcus, M. Scheffler, Phys. Rev. Lett. **78**, 3892 (1997)
166. P.M. Marcus, F. Alippi, Phys. Rev. B **57**, 1971 (1998)
167. Y. Mishin, D. Farkas, M.J. Mehl, D.A. Papaconstantopoulos, Phys. Rev. B **59**, 3393 (1999)
168. L.G. Wang, M. Sŏb, Phys. Rev. B **60**, 844 (1999)
169. F. Jona, P.M. Marcus, Phys. Rev. B **63**, 094113 (2001)
170. Y. Tian, F. Jona, J. Phys.: Condens Matter **13**, 094113 (2001); F. Jona, P.M. Marcus, Phys. Rev. B **66**, 094104 (2002)
171. M. Friák, M. Šob, V. Vitek, Phys. Rev. B **63**, 052405 (2001)
172. Y. Mishin, M.J. Mehl, D.A. Papaconstantopoulos, A.F. Voter, J.D. Kress, Phys. Rev. B **63**, 224106 (2001)
173. F. Jona, P.M. Marcus, Phys. Rev. B **65**, 155403 (2002)
174. X.Z. Ji, F. Jona, P.M. Marcus, Phys. Rev. B **68**, 075421 (2003)
175. L.G. Wang, M. Šob, Zhenyu Zhang, J. Phys. Chem. Solids **64**, 863 (2003)
176. M. Ćerny, M. Šob, J. Pokluda, P. Śandera, J. Phys.: Condens Matter **16**, 1045 (2004)
177. M.J. Mehl, A. Aguayo, L.L. Boher, R. de Coss, Phys. Rev. B **70**, 014105 (1991)
178. Y. Chen, C.-L. Fu, K.-M. Ho, B.B. Harmon, Phys. Rev. B **31**, 6775 (1985)
179. W.A. Bassett, E. Huang, Science **238**, 780 (1987)
180. Y. Chen, K.M. Ho, B.N. Harmon, Phys. Rev. B **37**, 283 (1988)

181. M. Ekman, B. Sadigh, K. Einarsdotter, P. Blaha, Phys. Rev. B **58**, 5296 (1998)
182. V. Paidar, L.G. Wang, M. Šob, V. Vitek, Modelling Simul. Mater. Sci. Eng. **7**, 369 (1999)
183. Many studies have shown that the bcc (or bct) phase of close-packed (fcc or hcp) metals is not metastable even when some tetragonal structures appearing on the Bain transformation path are related to energy minima [177]. They cannot be stabilised in the form of thin films [177], not even by a constraint imposed by the substrate (except for the beginning of the growth, i.e. up to the thickness of 2 or 9 monolayers [172,184,185])
184. T. Deutsch, P. Bayle, F. Lancon, J. Thibault, J. Phys.: Condens Matter **7**, 6407 (1995)
185. T. Deutsch, J. Thibault, J. Phys.: Condens Matter **15**, 1813 (2003)
186. E. Hüger, K. Osuch, M. Šob, in preparation
187. L.A. Bruce, H. Jaeger, Phil. Mag. A **37**, 337 (1978)
188. L.A. Bruce, H. Jaeger, Phil. Mag. A **40**, 97 (1979)
189. Theoretical studies have shown that the hcp structure is a metastable phase of metals with the fcc native structure [190]. This means that there exists an energy barrier in all transformation paths which connects the hcp with the fcc phase [120,138,191]
190. J. Jona, P.M. Marcus, J. Phys.: Condens. Matter **16**, 5199 (2004)
191. D. Roundy, C.R. Krenn, M.L. Cohen, J.W. Morris Jr., Phys. Rev. Lett. **82**, 2713 (1999)
192. M.J. Mehl, D.A. Papaconstantopoulos, N. Kioussis, M. Herbranson, Phys. Rev. B **61**, 4894 (2000)
193. N. Bernstein, E.B. Tadmor, Phys. Rev. B **69**, 094116 (2004)
194. W. Wulfhekel, T. Gutjahr-Löser, F. Zavaliche, D. Sander, J. Kirschner, Phys. Rev. B **64**, 144422 (2001)
195. Th. Duden, thesis (TU-Clausthal, 1996); Th. Duden, R. Zdyb, M.S. Altman, E. Bauer, Surf. Sci. **480**, 145 (2001)
196. E. Hüger, K. Osuch, in preparation
197. J. Dekoster, E. Jêdryka, C. Mény, G. Langouche, Europhys. Lett. **22**, 433 (1993)
198. F. Xu, J.J. Joyce, M.W. Ruckman, H.-W. Chen, F. Boscherini, D.M. Hill, S.A. Chambers, J.H. Weaver, Phys. Rev. B **35**, 2375 (1987)
199. A.Y. Liu, D.J. Singh, J. Appl. Phys. **73**, 6189 (1993)
200. L. Duo, R. Bertacco, G. Isella, F. Ciccacci, M. Richter, Phys. Rev. B **61**, 15294 (2000)
201. R. Bertacco, G. Isella, L. Duo, F. Ciccacci, A. di Bona, P. Luches, S. Valeri, Surf. Sci. **454-456**, 671 (2000)
202. S. Ram, Acta Materialia **49**, 2297 (2001)
203. S. Ram, D. Gosh, S.K. Roy, J. Material Science **36**, 3745 (2001)
204. C. Rath, J.E. Prieto, S. Muller, R. Miranda, K. Heinz, Phys. Rev. B **55**, 10791 (1997)
205. W. Donner, N. Metoki, A. Abromeit, H. Zabel, Phys. Rev. B **48**, 14745 (1993)
206. N. Metoki, W. Donner, H. Zabel, Phys. Rev. B **49**, 17351 (1994)
207. P. Boher, F. Giron, P. Houdy, P. Beauvillain, C. Chappert, P. Veillet, J. Appl. Phys. **70**, 5507 (1991)
208. M. El-Batanouny, M. Strongin, Phys. Rev. B **31**, 4798 (1985)
209. H. Kung, Y.-C. Lu, A.J. Griffin, Jr., M. Nastasi, T.E. Mitchell, J.D. Embury, Appl. Phys. Lett. **71**, 2103 (1997)